Earth-Science Reviews 237 (2023) 104306

Contents lists available at ScienceDirect

Earth-Science Reviews

journal homepage: www.elsevier.com/locate/earscirev

Environmental controls on very high $\delta^{238}U$ values in reducing sediments: Implications for Neoproterozoic seawater records

Matthew O. Clarkson [a,*], Tim C. Sweere [a,*], Chun Fung Chiu [a], Rick Hennekam [b], Fred Bowyer [c], Rachel A. Wood [a,c]

[a] Department of Earth Sciences, ETHZ, Zurich 8092, Switzerland
[b] Department of Ocean Systems, NIOZ Royal Netherlands Institute for Sea Research, 't Horntje 1797 SZ, the Netherlands
[c] School of GeoSciences, University of Edinburgh, James Hutton Road, Edinburgh EH9 3FE, UK

ARTICLE INFO

Keywords:
Ediacaran
Tonian
Uranium
Molybdenum
Sapropels
Metal Isotopes

ABSTRACT

Uranium isotopes ($\delta^{238}U$) are a widely applied tool for tracing global changes in oceanic anoxia. Interpretation of seawater values and trends, often reconstructed from carbonates, requires knowledge of the U isotope fractionation that occurs during U reduction, typically favouring the heavier ^{238}U isotope relative to ^{235}U. Yet the environmental controls on the expression of isotope enrichment during reduction ($\Delta^{238}U_{anox}$) are poorly understood, leading to large uncertainties in interpretation of seawater records. This is particularly limiting for the Neoproterozoic, where exceptionally low inferred seawater $\delta^{238}U$ requires very high $\Delta^{238}U_{anox}$, which are rarely seen in modern sediments. Here we present a compilation of authigenic $\delta^{238}U$ from modern and recent (Mediterranean sapropel) reducing settings to better constrain the first order controls on the expression of large U isotope enrichments. Accompanying geochemical data help identify the dominant mechanisms responsible for high $\Delta^{238}U_{anox}$, suggesting they are an expression of limited sedimentary U reduction in weakly euxinic settings or temporally dynamic reducing environments. Such environments are characterised by lower to intermediate organic carbon and uranium accumulation rates (OCAR, UAR) where U reduction appears dominated by non-diffusion-limited processes at the sediment-water interface, on sinking organic matter or within the water column itself. Conversely, under strongly euxinic conditions with higher OCAR and UAR, U reduction occurs mainly under a diffusion-limited regime in the sediment. These findings suggest that the very low seawater $\delta^{238}U$ of the Neoproterozoic may be a result of progressive ocean oxygenation and temporally dynamic expansions of anoxia, or the development of weakly euxinic conditions, rather than more widespread or 'intense' anoxia as previously inferred. Such a revised interpretation is more consistent with other geochemical and paleontological records from this time and is critical for understanding the relationship of anoxia to the rise of complex life.

1. Introduction

Seawater uranium isotope records ($\delta^{238}U_{sw}$), primarily reconstructed from carbonate ($\delta^{238}U_{carb}$) archives, have provided detailed insights into the magnitude and timing of global expansions of oceanic anoxia for many major transition and perturbations events in Earth history. The utility of U isotopes as a redox tracer stems from the fact that the largest isotope fractionation occurs during reduction and has a strong leverage on the global isotope mass balance (Andersen et al., 2017). Typically, U is reduced from soluble U(VI) to insoluble U(IV) which preferentially favours ^{238}U relative to ^{235}U in the insoluble phase (e.g. Stirling et al., 2015; Stylo et al., 2015; Brown et al., 2018). Given that the majority of anoxic U removal occurs within the sediment rather than the water column (McManus et al., 2006), and because of the long residence time of U in the modern ocean (320–560 kyrs; Dunk et al., 2002), $\delta^{238}U_{sw}$ can track global changes in the areal extent of seafloor anoxia. Indeed, negative $\delta^{238}U_{carb}$ excursions are associated with numerous Phanerozoic deoxygenation events, including mass extinction intervals (Fig. 1; e.g. Jost et al., 2017; Clarkson et al., 2018; Zhang et al., 2018a). Proterozoic $\delta^{238}U_{carb}$ records further document multi-million-year fluctuations,

Abbreviations: TOC, Total Organic Carbon; PNU, Particulate Non-lithogenic Uranium; BAR, Burial Accumulation Rate; MoAR, Molybdenum Accumulation Rate; UAR, Uranium Accumulation Rate; UCC, Upper Continental Crust; PAAS, Post Archaean Average Shale; OAE, Oceanic Anoxic Event.

* Corresponding authors.
E-mail addresses: matthewc@ethz.ch (M.O. Clarkson), tim.sweere@erdw.ethz.ch (T.C. Sweere).

https://doi.org/10.1016/j.earscirev.2022.104306
Received 14 June 2022; Received in revised form 15 November 2022; Accepted 26 December 2022
Available online 3 January 2023

potentially tracking ocean oxygenation events in an otherwise predominantly anoxic ocean (Fig. 1; Lau et al., 2017; Zhang et al., 2018c; Tostevin et al., 2019; Wei et al., 2021; Zhang et al., 2022).

Regardless of time period, quantitative interpretation of $\delta^{238}U_{sw}$ in terms of the size of anoxic sinks and the areal extent of seafloor anoxia requires assumption of the magnitude of U isotope fractionation that occurs in anoxic sediments (i.e. the difference between reduced authigenic $\delta^{238}U$ and aqueous dissolved $\delta^{238}U$; $\Delta^{238}U_{anox}$). However, the relationship of $\Delta^{238}U_{anox}$ to environmental and depositional controls, including ambient redox conditions, is poorly understood in the modern ocean (e.g. Lau et al., 2020; Lau et al., 2022), making it difficult to estimate for ancient applications. Experimental and theoretical studies suggest a $\Delta^{238}U_{anox}$ of ~ +1.2–1.4‰ associated with the precipitation of U(IV) as a result of the nuclear field shift effect (Abe et al., 2008; Basu et al., 2014; Stirling et al., 2015; Stylo et al., 2015; Brown et al., 2018). In modern anoxic sediments, however, U reduction primarily occurs within the sediment pile, creating a first order diffusion-limitation on isotope enrichment and hence a smaller expression of $\Delta^{238}U_{anox}$, with a theoretical maximum effective $\Delta^{238}U_{anox}$ that is half of the full enrichment factor (i.e. ~ +0.6‰; Clark and Johnson, 2008; Andersen et al., 2014; Lau et al., 2020). The importance of diffusion-limitation for anoxic U burial in the modern ocean is evident from an inferred global average $\Delta^{238}U_{anox}$ of +0.4 ± 0.1‰ based on isotope mass balance calculations (Andersen et al., 2017). For interpretations of paleo-datasets, however, it is common to use a $\Delta^{238}U_{anox}$ between +0.4 and + 0.8‰, based on the values observed in modern anoxic sediments, but this range results in large uncertainties for estimates of the areal extent of anoxia (e.g. Jost et al., 2017; Lau et al., 2017; Clarkson et al., 2018; Zhang et al., 2020b). Thus, knowledge on the controls of $\Delta^{238}U_{anox}$ is a severe limitation for the quantitative application of $\delta^{238}U$ as a geochemical tracer.

The Neoproterozoic carbonate $\delta^{238}U$ records pose a particular challenge for interpretation using isotope mass balance models and the diffusion-limitation framework. Specifically, two intervals of exceptionally low $\delta^{238}U_{sw}$ are inferred for the early Tonian and late Ediacaran (Fig. 1, down to ~ −1.2‰; Zhang et al., 2018c; Zhang et al., 2022) which are markedly lower than other negative $\delta^{238}U_{sw}$ excursions of the Proterozoic and early Paleozoic (around −0.9‰, Fig. 1; Lau et al., 2017; Dahl et al., 2019; Wei et al., 2021). Note that the lowermost carbonate $\delta^{238}U$ values are used here to infer $\delta^{238}U_{sw}$ as carbonates are often positively offset from seawater due to early diagenesis (Romaniello et al., 2013). These extreme Neoproterozoic $\delta^{238}U_{sw}$ excursions appear to be long lived (>0.5 Myrs), so are unlikely to be the result of a dynamic U cycle response that is predicted for Phanerozoic perturbation events (see Zhang et al., 2020b; Kipp and Tissot, 2022 for discussion on dynamic models). Instead, the Neoproterozoic $\delta^{238}U_{sw}$ excursions are suggested to reflect a larger expression of $\Delta^{238}U_{anox}$ (Wei et al., 2021; Zhang et al., 2022). This requirement is illustrated using a simple steady-state two-sink model describing the relationship of $\delta^{238}U_{sw}$ to the

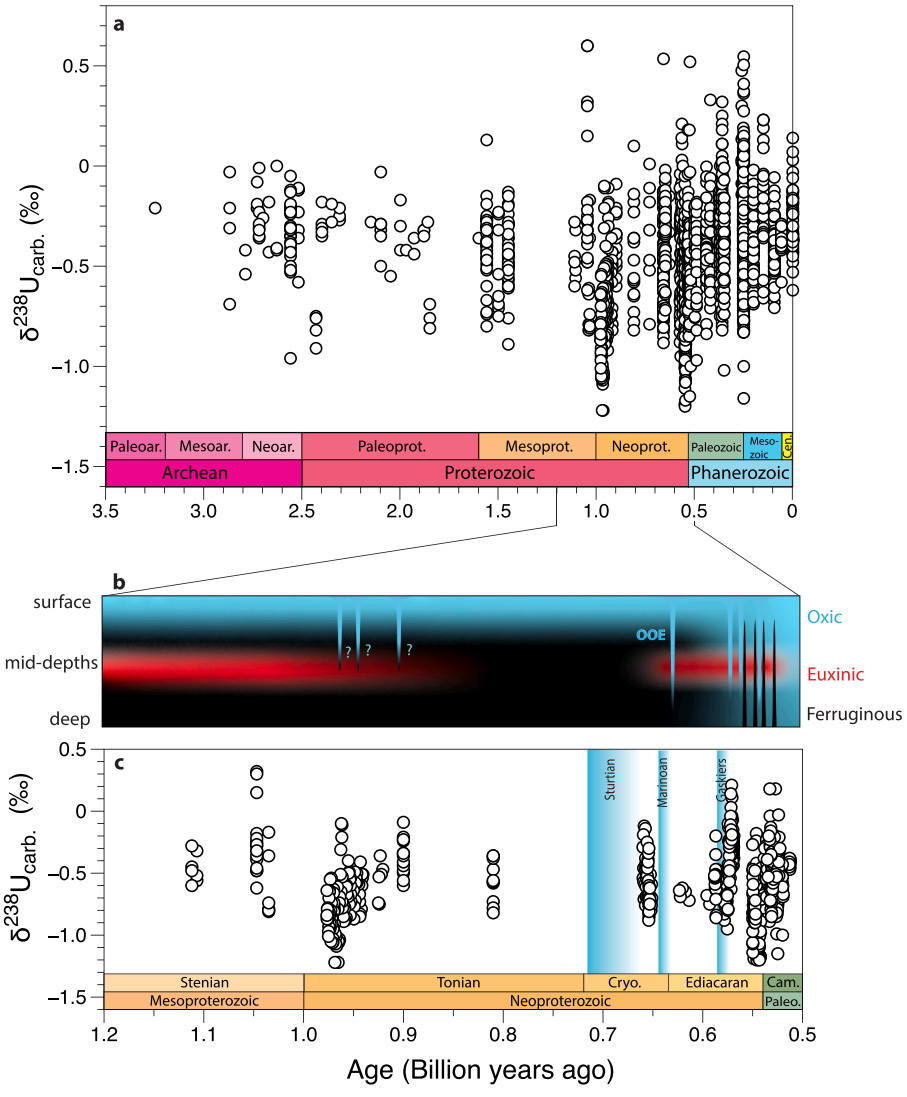

Fig. 1. Summary of carbonate $\delta^{238}U$ through time. **a** published carbonate $\delta^{238}U$ records updated from Chen et al. (2021) from original sources (Brennecka et al., 2011a; Romaniello et al., 2013; Dahl et al., 2014; Azmy et al., 2015; Hood et al., 2016; Lau et al., 2016; Dahl et al., 2017; Elrick et al., 2017; Jost et al., 2017; Lau et al., 2017; Song et al., 2017; Bartlett et al., 2018; Chen et al., 2018; Clarkson et al., 2018; Herrmann et al., 2018; Wei et al., 2018; White et al., 2018; Zhang et al., 2018a; Zhang et al., 2018b; Zhang et al., 2018c; Dahl et al., 2019; Gilleaudeau et al., 2019; Tostevin et al., 2019; Zhang et al., 2019; Brüske et al., 2020a; Cao et al., 2020; Cheng et al., 2020; del Rey et al., 2020; Li et al., 2020; Zhang et al., 2020a; Zhang et al., 2020c; Clarkson et al., 2021b; Chen et al., 2022; Zhang et al., 2022). **b** Schematic of late Proterozoic ocean redox dynamics modified from Wood et al. (2019) and references therein, based on local and global redox records. Note that euxinia after ~645 Ma was restricted to South China and was highly intermittent (Li et al., 2010; Och et al., 2016; Bowyer et al., 2017). Ocean Oxygenation Events (OOEs) in the early Tonian are inferred from higher values in the carbonate $\delta^{238}U$ record (Zhang et al., 2022) but have not yet been identified with local tracers. These records indicate progressive oxygenation in the late Neoproterozoic and changes in the occurrence of anoxic ferruginous (non-sulfidic) and euxinic (sulfidic) conditions. **c** Higher resolution plot of Mesoproterozoic to Cambrian published carbonate $\delta^{238}U$ records with updated age models (see Table S2; after Yang et al., 2021; Bowyer et al., 2022). Distinctly low $\delta^{238}U_{carb}$ values are seen in the early Tonian and late Ediacaran compared to Mesoproterozoic, mid-Neoproterozoic and Paleozoic.

fraction of U buried in anoxic sinks (F_{anox}) assuming different $\Delta^{238}U_{anox}$ values (Fig. 2):

$$\delta^{238}U_{sw} = \delta^{238}U_{riv} - (F_{anox} * \Delta^{238}U_{anox}) - (F_{other} * \Delta^{238}U_{other}) \quad (1)$$

where riverine $\delta^{238}U$ ($\delta^{238}U_{riv}$) = −0.3‰ (Upper Continental Crust; UCC) and F_{other} is the fraction of non-anoxic sinks (including Mn-oxides and hydrothermal sinks) with an average $\Delta^{238}U_{other}$ = +0.03‰ (Andersen et al., 2017). This exercise demonstrates that a $\delta^{238}U_{sw}$ value of −0.9‰, e.g. inferred for the Cryogenian (Lau et al., 2017), can be explained with an average $\Delta^{238}U_{anox}$ of ~ +0.6‰ relative to seawater, but requires that all U is buried in anoxic sinks (Fig. 2). This is plausibly explained using the diffusion-limitation framework and a fully anoxic ocean. By contrast, the early Tonian and late Ediacaran $\delta^{238}U_{sw}$ minima are only compatible with a $\Delta^{238}U_{anox}$ above +0.9‰ and even larger values are plausible assuming that non-anoxic U sinks were also present.

This simple illustrative model assumes riverine U inputs had a similar $\delta^{238}U_{riv}$ to the UCC as is seen in modern rivers (Noordmann et al., 2015a; Noordmann et al., 2015b; Andersen et al., 2016). It is unlikely that the very negative Neoproterozoic $\delta^{238}U_{sw}$ values reflect changes in $\delta^{238}U_{riv}$, as weathering processes only induce minor isotope fractionation and there is no significant $\delta^{238}U$ variation for the main crustal rock types or for different crustal ages (Noordmann et al., 2015a; Noordmann et al., 2015b; Andersen et al., 2016; Andersen et al., 2017). Bruske et al. (2020a) hypothesised that terrestrial weathering in a mildly oxidative atmosphere could produce leaching artefacts, resulting in lower $\delta^{238}U_{riv}$ in the early Paleoproterozoic. However, as a more oxidized atmosphere was established during the Great Oxidation Event (2.45–2.32 Ga) such weathering related fractionations were deemed insignificant for the remainder of the Proterozoic (Brüske et al., 2020a). Major changes in the size of hydrothermal sinks, which also favour ^{238}U relative to ^{235}U, can further be discounted as an explanation for the extremely low $\delta^{238}U_{sw}$ values since the magnitude of isotope fractionation caused by hydrothermal alteration of oceanic crust is i) minor in the modern ocean (+0.15‰; Andersen et al., 2017) and ii) thought to only be significant in an oxidized ocean (Andersen et al., 2015). Thus, a higher $\Delta^{238}U_{anox}$ is the most plausible reason to explain exceptionally low Neoproterozoic $\delta^{238}U_{sw}$ values.

The reasons for such high inferred $\Delta^{238}U_{anox}$ values are not clear. Following earlier explanations (Andersen et al., 2017; Andersen et al., 2020) it is suggested that the very low late Ediacaran $\delta^{238}U_{sw}$ values are indicative of non-diffusion-limited U reduction on a global scale, occurring within an organic floc at the sediment water interface or within the water column (Wei et al., 2021). Late Ediacaran $\delta^{238}U_{sw}$ values are thus interpreted as indicating more 'intense' anoxia than earlier and later intervals and imply an even greater area of seafloor anoxia (Wei et al., 2021). As a result, it was suggested that these anoxic expansions induced intervals of significant biodiversity reduction or turnover in early metazoans (Zhang et al., 2018c; Wei et al., 2021). This interpretation, however, presents a paradox, as other global redox tracers, including molybdenum ($\delta^{98}Mo$) and selenium isotopes ($\delta^{82/76}Se$), show progressively more oxygenated conditions during the late Neoproterozoic (see summary in Fig. 1; Chen et al., 2015; Pogge von Strandmann et al., 2015) and multiple Ocean Oxygenation Events (OOEs; Sahoo et al., 2016). Moreover, local redox records from in-situ proxies such as Fe-speciation, cerium anomalies and I/Ca, demonstrate that anoxia during this time interval was extremely spatially, temporally and chemically dynamic (Fig. 1; Li et al., 2010; Wood et al., 2015; Och et al., 2016; Tostevin et al., 2016; Bowyer et al., 2017; Tostevin and Mills, 2020) with no clear global uniform expansion of anoxia in shallow marine sediments or correlation to biodiversity. Less is known about local redox dynamics for the early Tonian. Zhang et al. (2022) use the $\delta^{238}U_{sw}$ record to infer non-diffusion-limited U reduction associated with organic matter in the water column and hence the expansion of anoxia into shallow waters, linked to high productivity.

To better understand the environmental controls on large expressions of $\Delta^{238}U_{anox}$ we examine authigenic $\delta^{238}U$ ($\delta^{238}U_{auth}$) systematics in modern and recent (Mediterranean sapropels S1 to S9) reducing sediments using a combination of new and published data. Additionally, we use water column sulfide concentrations, authigenic molybdenum isotopes ($\delta^{98}Mo_{auth}$), Mo and U enrichment factors (MoEF & UEF), metal accumulation rates and organic carbon accumulation rates to better characterise the redox environments. In doing so, we identify those conditions conducive to higher $\Delta^{238}U_{anox}$ values. Contrary to previous suggestions (Wei et al., 2021; Zhang et al., 2022), we ascertain that higher $\Delta^{238}U_{anox}$ are more typical of less-reducing localities, at lower H_2S concentrations close to the chemocline, and those with temporally variable anoxia. If these findings are applicable to the Neoproterozoic, this suggests that the very negative $\delta^{238}U_{sw}$ values might be better

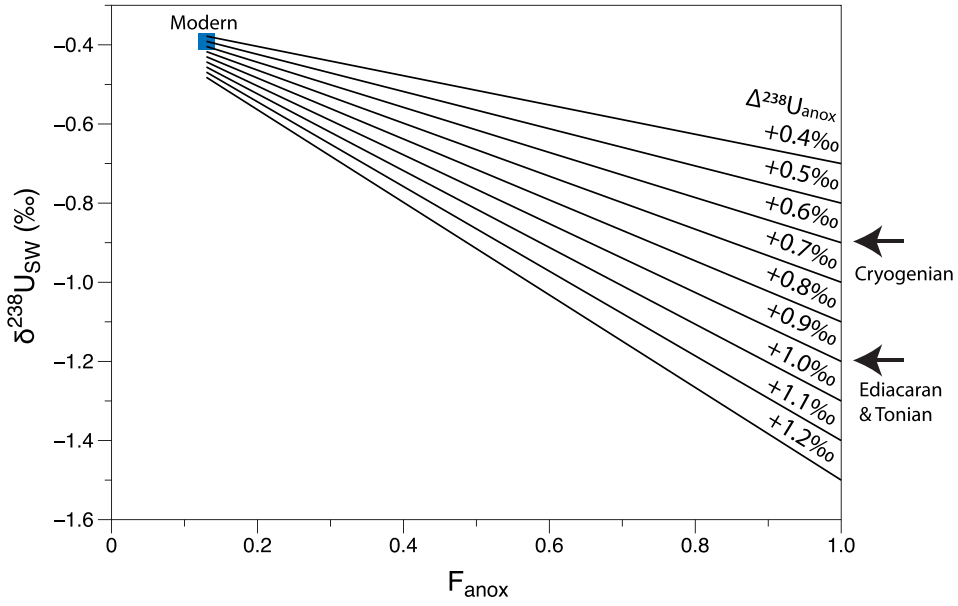

Fig. 2. Two-sink U isotope mass balance model. Illustrates the range of plausible $\Delta^{238}U_{anox}$ values required to generate given $\delta^{238}U_{sw}$ values as a function of the fraction of anoxic sedimentary U sinks relative to total U sinks (F_{anox}). Arrows refer to $\delta^{238}U_{sw}$ minima that can be explained by a fully anoxic ocean with varying $\Delta^{238}U_{anox}$. Note that $\delta^{238}U_{carb.}$ minima are interpreted to be closest to seawater but may be positively offset due to early diagenesis (Romaniello et al., 2013).

interpreted as being a consequence of the progressive oxidation of the oceans and the temporally dynamic redoxcline indicated by local redox proxies, or the development of weakly euxinic conditions driven by secular changes in global iron-sulfate dynamics.

2. Materials and methods

We present a compilation of modern and recent $\delta^{238}U_{auth}$ and authigenic U concentrations ($[U_{auth}]$) (Table S3) derived from bulk measurements on reducing sediments. We separate samples based on the predominant environmental setting, but acknowledge there may be some overlap, for example upwelling sites might also include data from the hypoxic edges of the oxygen minimum zone (Bruggmann et al., 2021). The modern anoxic sediment dataset is restricted to samples where Al concentrations were reported in the original publication, allowing for calculation of $[U_{auth}]$ and $\delta^{238}U_{auth}$ values following previously described methods (Chiu et al., 2022). Where Al is not reported or another detrital element used for correction, we use reported $\delta^{238}U_{auth}$, but do not include those studies that only report bulk $\delta^{238}U$. For consistency and owing to the range of detrital compositions commonly used in the literature for detrital corrections, we calculated $\delta^{238}U_{auth}$ using detrital U/Al ($U/Al_{detrital}$) of the Upper Continental Crust (UCC = 0.35 ppm/wt% and a $\delta^{238}U_{detrital}$ of −0.3‰ Taylor and McLennan, 1985, McLennan, 2001, Andersen et al., 2017). UCC has a similar U/Al value to Post Archaean Average Shale (PAAS; $U/Al_{detrital}$ = 0.31; Taylor and McLennan, 1985) which is also commonly used. Note that a lower U/Al value of 0.11 has been used in the literature, cited as PAAS based on a publication error in Tribovillard et al. (2006) which in fact reflects the average continental crust (i.e. upper and lower continental crust; Taylor and McLennan, 1985; McLennan, 2001). In support of this approach, the UCC $U/Al_{detrital}$ appears to fit well with U/Al relationships for the global compilation (Fig. S1). For the Black Sea we use a range of local $U/Al_{detrital}$ estimates (0.31–0.37) based on the suspended load of Turkish rivers and sediments from the Danube (Yiğiterhan and Murray, 2008). This value is similar to UCC and results in larger detrital corrections and notably higher $\delta^{238}U_{auth}$ than previously estimated ($U/Al_{detrital}$ = 0.18; Montoya-Pino et al., 2010; Andersen et al., 2014; Rolison et al., 2017; Brüske et al., 2020b) but is likely more accurate. For the Black Sea samples, we propagate the uncertainty in $U/Al_{detrital}$ using a Monte-Carlo approach assuming a uniform range in detrital compositions (Table S3). Where available, $\delta^{98}Mo_{auth}$ are also included in the compilation, where we use originally reported $\delta^{98}Mo_{auth}$ values owing to greater consistency in $Mo/Al_{detrital}$ estimates in the literature.

New and published sapropel data (see Table 1, S3 & S4) come from two localities in the Eastern Mediterranean; namely ODP Site 967 (Andersen et al., 2020) and Site 46PE406-E1 (Clarkson et al., 2021a; Sweere et al., 2021; Chiu et al., 2022). Calculated $\delta^{238}U_{auth}$, $\delta^{98}Mo_{auth}$ and enrichment factor data follow previously described methods (Chiu et al., 2022). We use local $U/Al_{detrital}$ of 0.26 and $Mo/Al_{detrital}$ of 0.2 (ppm/wt%) for all sapropel samples constrained using non-sapropel sediments at Site 46PE406-E1 (Clarkson et al., 2021a; Chiu et al., 2022). Note that for the most recent anoxic interval (sapropel S1) at Site 46PE406-E1 we use $\delta^{238}U_{auth}$ from carbonate leachates because they more precisely record authigenic values compared to detritus corrected bulk measurements at low U concentrations (Clarkson et al., 2021a). For these samples, $[U_{auth}]$ data are calculated using $\delta^{234}U$, which can give an estimate of the detrital fraction in younger sediments (see Andersen et al., 2014; Holmden et al., 2015), but are within error of estimates using U/Al (Clarkson et al., 2021a). Note that estimated $[U_{auth}]$ are likely lower than true depositional $[U_{auth}]$ in some S1 samples, because post-depositional oxidative diagenesis caused U loss (Clarkson et al., 2021a). Total organic carbon (TOC) data are presented for all sapropel samples from Site 46PE406-E1 following previously described methods (Table S4; Chiu et al., 2022).

The modern and sapropel $\delta^{238}U_{auth}$ data are shown as a function of $[U_{auth}]$ in Fig. 2. We also summarise the distribution of $\Delta^{238}U_{anox}$ per environment ($\delta^{238}U_{auth}$-$\delta^{238}U_{aq}$), calculated using modern seawater (−0.39‰; Andersen et al., 2017) or water column data for $\delta^{238}U_{aq}$ (Black Sea; Bruske et al., 2020, Lake Pavin; Cole et al., 2020) in Fig. 3. For sapropels we use the global seawater value to calculate $\Delta^{238}U_{anox}$, acknowledging that this leads to a minor decrease in $\Delta^{238}U_{anox}$ for the samples from the upper part of S5 which may have experienced bottom water U depletion (Andersen et al., 2018; Chiu et al., 2022). We also calculate the U-abundance weighted average $\Delta^{238}U_{anox}$ of each depositional environment to account for the range of U enrichments seen in each locality, and to better understand the leverage of different reducing environments on global U isotope mass balance. The abundance weighted average $\Delta^{238}U_{anox}$ is calculated for each environment and for the global dataset:

$$\Sigma\left(\Delta^{238}U_{anox}{}^{*}\left([U]_{auth}/\Sigma[U]_{auth}\right)\right) \quad (2)$$

where $\Sigma[U]_{auth}$ is the sum of $[U_{auth}]$ for all samples from that environment.

For Site 46PE406-E1, linear sedimentation rates are calculated using previously published age models (Grant et al., 2016; Sweere et al., 2021) and combined with dry bulk densities to calculate bulk accumulation rates (BAR). Accumulation rates for Mo, U (MoAR and UAR) and organic carbon (OCAR) were then calculated by multiplying concentrations by BAR and expressed as $ng/cm^2/yr$ and $g/m^2/yr$, respectively, to facilitate comparison to modern environments.

Table 1
Summary of data sources.

Classification		Location	Reference
Modern	Euxinic	Black Sea Basin	Andersen et al. (2014); Bruske et al. (2020); Rolison et al. (2017); Montoya-Pino et al. (2010)
		Black Sea Chemocline	Andersen et al. (2014); Bruske et al. (2020)
		Black Sea Unit II	Montoya-Pino et al. (2010); Bruske et al. (2020)
		Cariaco Basin	Andersen et al. (2014); Bruske et al. (2020)
		Kyllarren Fjord	Noordmann et al. (2015)
		Landsort Deep	Noordmann et al. (2015)
	Hypoxic	Toulon Bay	Dang et al. (2018)
		Washington Margin	Andersen et al. (2016)
	Upwelling	Peru Margin	Bruggmann et al. (2021); Weyer et al. (2008)
		Namibia Margin	Abshire et al. (2020); He et al. (2021)
	Ferruginous	Lake Pavin, Lake Brownie	Cole et al. (2020)
	Mixed	NZ Fjords	Hinojosa et al. (2016)
Sapropel	S1, S5	ODP Site 967	Andersen et al. (2018, 2020)
	S1	Site 46PE406-E1	Clarkson et al. (2021); This study
	S5, S7	Site 46PE406-E1	Sweere et al. (2020); Chui et al. (2022)
	S3, 4, 6, 8, 9	Site 46PE406-E1	Sweere et al. (2020); This study

3. Results

3.1. Modern compilation

3.1.1. Overview

The data compilation demonstrates important differences in the magnitude and variability of U isotope fractionation as a function of $[U_{auth}]$ and depositional environment (Fig. 3). The vast majority of samples show higher $\delta^{238}U_{auth}$ than modern seawater (−0.39‰), indicative of the enrichment of ^{238}U, relative to ^{235}U, in the reduced authigenic phase (Weyer et al., 2008; Montoya-Pino et al., 2010; Andersen et al., 2014; Noordmann et al., 2015b; Rolison et al., 2017;

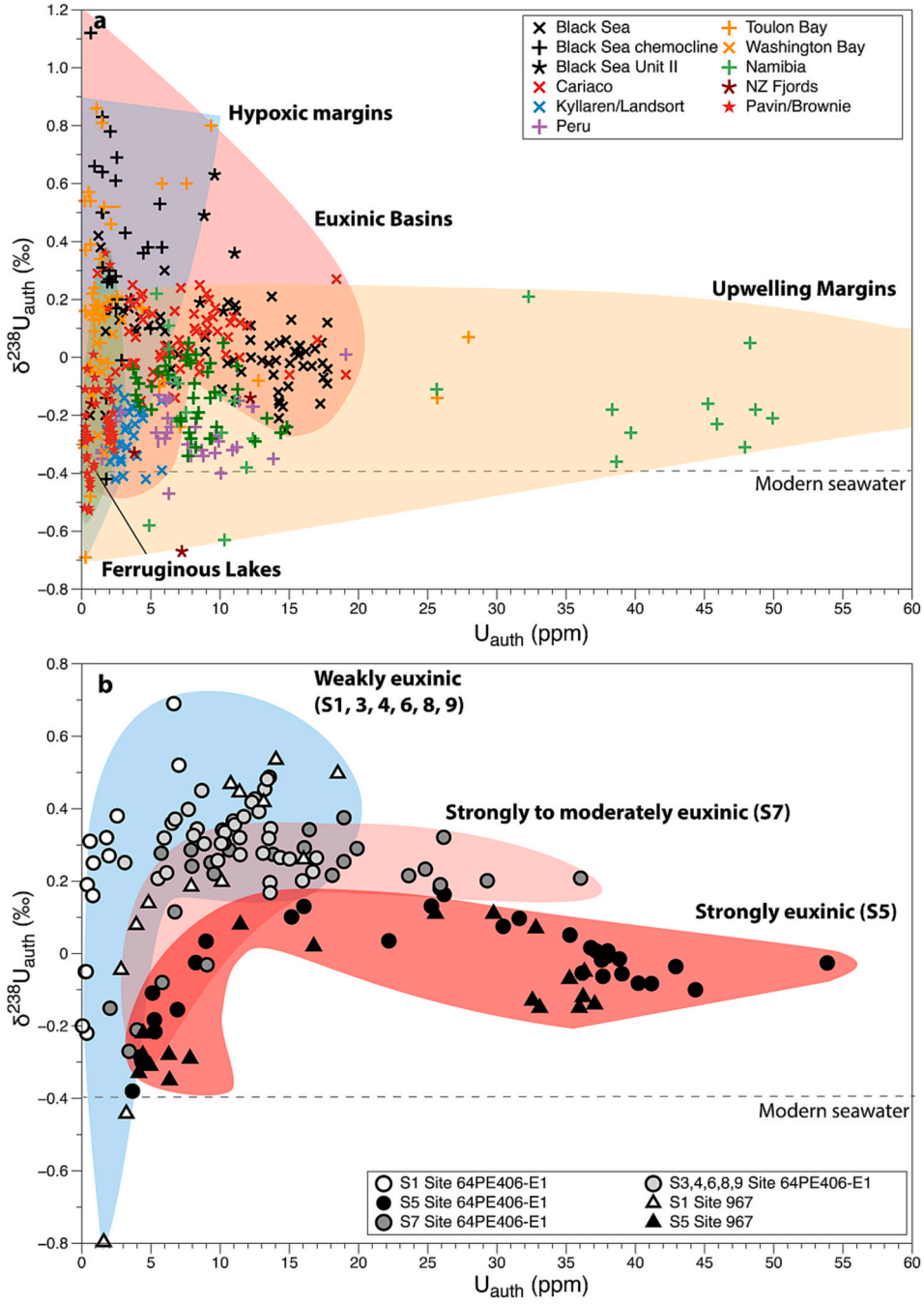

Fig. 3. Compilation of modern (a) and sapropel (b) $\delta^{238}U_{auth}$ values. Figure limited to 60 ppm U_{auth} for clarity, excluding two samples from Namibia. Degree of euxinia in **b** is qualitatively estimated based on δ^{98}Mo and MoEF–UEF (see section 3.2.1) in the same samples and refers to peak sapropel conditions (Sweere et al., 2021; Chiu et al., 2022).

Brüske et al., 2020b). Most samples have $\delta^{238}U_{auth}$ below ~ +0.8‰, supporting a maximum $\Delta^{238}U_{anox}$ of ~ +1.2‰ in natural sediments (Andersen et al., 2014). One sample from the Black Sea chemocline has higher $\delta^{238}U_{auth}$ although this estimate has larger uncertainty based on the range of local $U/Al_{detrital}$ estimates for the Black Sea (Table S4). Despite great variability, the U-abundance weighted average $\Delta^{238}U_{anox}$ of global marine samples is calculated as +0.4‰ (Fig. 4), in excellent agreement with estimates from global mass balance calculations (0.4 ± 0.1‰; Andersen et al., 2017) suggesting that the compiled database is representative of modern reducing U sinks.

A minority of samples have $\delta^{238}U_{auth}$ lower than modern seawater, possibly reflecting U adsorption to organic matter and authigenic metal oxide phases, or potentially an artefact of abiotic Fe-reduction (Brennecka et al., 2011b; Stylo et al., 2015; Hinojosa et al., 2016; Abshire et al., 2020; Cole et al., 2020). Little is known about the relative contributions of these isotopically light phases to reducing sediments, or the potential of these phases to mask the higher $\delta^{238}U_{auth}$ that is more typical of U reduction. Very low U concentrations have been observed in fresh planktic organic matter (~0.3 ppm; Holmden et al., 2015) and adsorption experiments required doping with U in order to make precise measurements (Chen et al., 2021), suggesting that the contribution to bulk reducing sediments should generally be small. That said, the U contributions of so-called particulate non-lithogenic U (PNU) to anoxic sediments can be significant (10–70%; Zheng et al., 2002) but this likely reflects a combination of reduced U(IV) and adsorbed U(VI), with higher and lower $\delta^{238}U_{auth}$ respectively. The U pool of dispersed metal oxides is

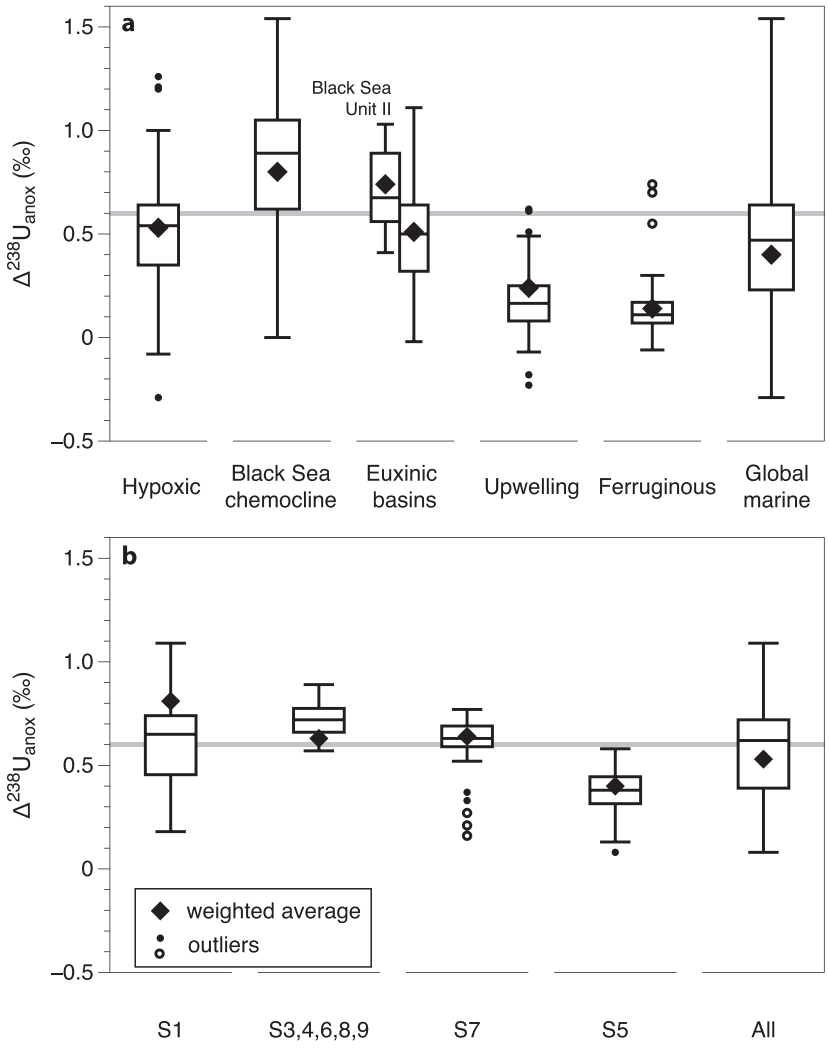

Fig. 4. Summary of U isotope systematics for different environments. Box-whisker plots used to summarise the distribution of $\Delta^{238}U_{anox}$ for modern reducing environments compared to the entire global database (**a**) and for sapropels from Site 46PE406-E1 (**b**). Outliers are defined as >1.5× interquartile range (IQR) (closed circles) and > 3× IQR (open circles). Uranium-abundance weighted average $\Delta^{238}U_{anox}$ (diamonds) are shown for comparison. Grey line demarks the diffusion-limited threshold of +0.6‰. Note that euxinic basins do not include the Black Sea chemocline data or Unit II.

likely small, with no clear dominance to the U budget of bulk sediments that show enrichments in Fe-Mn-oxide phases (Clarkson et al., 2020; Clarkson et al., 2021a). Uranium isotope fractionation linked to abiotic Fe reduction may involve kinetic processes that favour ^{235}U (Stylo et al., 2015), but even in ferruginous lake sediments only a few samples have negative $\Delta^{238}U_{anox}$ values (Cole et al., 2020). Further work is required to separate these competing U pools, and whilst the $\delta^{238}U_{auth}$ of some samples are dominated by such contributions (Fig. 3), given their relatively low [U_{auth}] we expect U accumulation via reduction, showing isotope fractionation due to the nuclear field shift effect, to be dominant for most of the sample set.

3.1.2. *Euxinic basins*

Permanent and temporary euxinic basins (Black Sea, Cariaco Basin, Landsort Deep and Kyrallen Fjord) are classic locations for studying the impact of redox-dependant processes on metal isotope systematics. For samples with low U enrichments and low $\delta^{238}U_{auth}$, U is likely near-quantitatively reduced in isolated porewaters (Lau et al., 2020). Progressive U enrichment under diffusion-limited conditions leads to a positive correlation of $\delta^{238}U_{auth}$ with [U_{auth}] up to ~10 ppm for all euxinic localities. At higher sedimentary [U_{auth}] in the Black Sea, $\delta^{238}U_{auth}$ decreases, thought to reflect bottom water U depletion and preferential removal of the heavy isotope via sedimentary reduction (Rolison et al., 2017; Brüske et al., 2020b). This feature is consistent with the water column $\delta^{238}U$ profile that shows a gradual decrease below the chemocline (Fig. 5). Some of the Black Sea data overlap with samples from modern hypoxic margins (see section 3.1.4), with lower U enrichments and much higher $\delta^{238}U_{auth}$. These samples are exclusively from the basin margin closest to the chemocline between 100 and 300 m water depth (Fig. 5). Comparing sedimentary $\delta^{238}U_{auth}$ with water column $\delta^{238}U$ (Fig. 5; Rolison et al., 2017; Brüske et al., 2020b), and hence accounting for bottom water U depletion, demonstrates that chemocline samples have the highest $\Delta^{238}U_{anox}$ (Figs. 4 & 5), within error of the full enrichment factor. Deeper in the basin, $\Delta^{238}U_{anox}$ remains approximately constant (Fig. 5). These depth dependant differences were not identified previously by Bruske et al. (2020b), who used a much lower $U/Al_{detrital}$ (0.18 ppm/wt%) compared to the local estimate from the Danube and Turkish rivers used here (0.31–0.37) or UCC (0.35), instead inferring relatively constant $\Delta^{238}U_{anox}$ for all samples. This highlights the importance of using local detrital values to obtain $\delta^{238}U_{auth}$. Similarly high $\delta^{238}U_{auth}$ values are seen in the Holocene Black Sea Unit II samples that mark the onset of euxinia in the basin (Fig. 3–5). For Unit II, $\Delta^{238}U_{anox}$ reaches up to ~ +1‰ (Montoya-Pino et al., 2010; Brüske et al., 2020b), assuming no significant effect of bottom water U depletion during deposition. For the seasonally euxinic Cariaco Basin (Fig. 3), $\delta^{238}U_{auth}$ are generally lower than the Black Sea, with a maximum around +0.2‰ ($\Delta^{238}U_{anox}$ ~ +0.6‰) but with a positive correlation between $\delta^{238}U_{auth}$ and [U_{auth}] (Andersen et al., 2014; Lau et al., 2017; Brüske et al., 2020b). In contrast to the Black Sea, Cariaco Basin samples do not show a clear negative correlation of $\delta^{238}U_{auth}$ and [U_{auth}] at

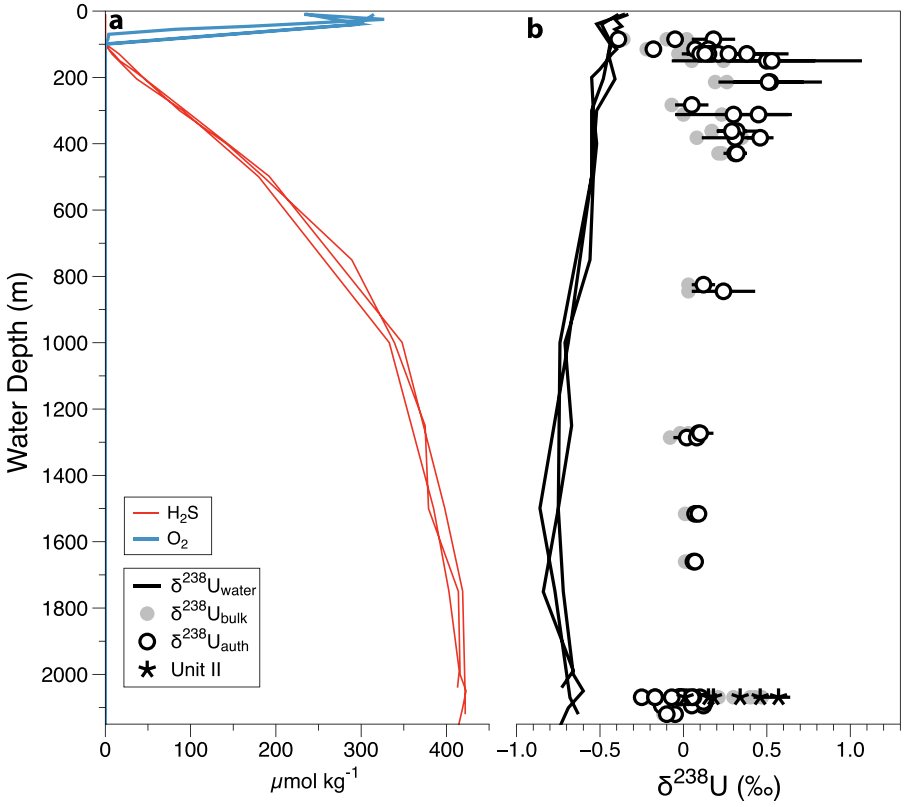

Fig. 5. Uranium isotope systematics for the Black Sea. a Water column dissolved O_2 and H_2S_{total} concentrations (Rolison et al., 2017). **b** Water column $\delta^{238}U$ (black lines) and core top sediment (<2 cm) $\delta^{238}U_{auth}$ (open circles) from different sediment-water interface depths sampled at the basin margins (Rolison et al., 2017; Brüske et al., 2020b). Grey data points are bulk measurement $\delta^{238}U$. Uncertainties (2SD) for $\delta^{238}U_{auth}$ are propagated errors using a Monte Carlo approach assuming a uniform distribution of local detrital U/Al estimates from Turkish and Danube river sediments (0.31–0.37; Yiğiterhan and Murray, 2008). Sampling depths for Unit II samples from Montoyo-Pino et al. (2010) are not reported so these depths were set to the same depth as Brüske et al. (2020).

higher concentrations, likely because U depletion in bottom waters is only ~10% of the U inventory (Andersen et al., 2014; Brüske et al., 2020b). The temporarily euxinic basins of Landsort Deep and Kyrallen Fjord (Noordmann et al., 2015b) show lower U enrichments and $\delta^{238}U_{auth}$ values, but in a trend that is consistent with other euxinic localities. Overall, euxinic basins show a wide range of $\Delta^{238}U_{anox}$ values, spanning the entire theoretical range. When the Black Sea chemocline and Unit II samples are excluded, the U-abundance weighted average $\Delta^{238}U_{anox}$ of euxinic basins is +0.5‰, close to the diffusion-limited threshold. By contrast, the U-abundance weighted average $\Delta^{238}U_{anox}$ of Black Sea chemocline samples is higher, at +0.8‰, and + 0.74‰ for the Unit II samples. Both are outside of the interquartile range for the euxinic basins as a whole (Fig. 4).

3.1.3. *Upwelling margins*

Data from modern upwelling margins, namely Peru and Namibia (Weyer et al., 2008; Abshire et al., 2020; Bruggmann et al., 2021; He et al., 2021), tend to overlap with euxinic basins, but with a larger range of $[U_{auth}]$ and more limited range of $\delta^{238}U_{auth}$, almost exclusively below +0.2‰ ($\Delta^{238}U_{anox} < +0.6$‰; Fig. 4). The highest $[U_{auth}]$ are from the upwelling centre near Luderitz in Namibia (up to 95 ppm; Abshire et al., 2020), whilst samples from the periphery of the upwelling zone further south tend to show lower U enrichments (He et al., 2021) and are similar to the Peru Margin (Weyer et al., 2008; Bruggmann et al., 2021). Some samples have $\delta^{238}U_{auth}$ closer to modern seawater despite very large U enrichments. These data are thought to reflect more quantitative U reduction in isolated porewaters as a result of high organic accumulation and U reduction rates (Lau et al., 2020). These lower $\delta^{238}U_{auth}$ values result in the weighted average $\Delta^{238}U_{anox}$ of +0.24‰ for upwelling settings, that is much lower than euxinic basins and the diffusion-limited threshold.

3.1.4. *Hypoxic and ferruginous settings*

Less reducing localities, represented by modern hypoxic settings, tend to show lower U enrichments with the largest range of $\delta^{238}U_{auth}$ values for any oceanographic setting (Fig. 3), reaching a maximum of +0.86‰, equivalent to $\Delta^{238}U_{anox}$ of ~1.2‰ and close to the full theoretical isotope enrichment factor (Andersen et al., 2016; Dang et al., 2018). Some samples from the Washington Margin show higher $[U_{auth}]$ and lower $\delta^{238}U_{auth}$ (<+0.2‰), more comparable to upwelling sites and likely reflecting temporarily more reducing conditions. Despite the large range in $\delta^{238}U_{auth}$ for hypoxic margins, the U-abundance weighted average $\Delta^{238}U_{anox}$ is ~ + 0.5‰. Samples from the New Zealand fjords (Hinojosa et al., 2016) capture a range of reducing conditions, from suboxic to anoxic, and generally show relatively muted $\delta^{238}U_{auth}$ values with a maximum of −0.16‰ for the largest U enrichment. Ferruginous sediments are poorly represented in the dataset and are exclusively from lake settings, but overlap with the hypoxic margin samples, showing a large variability in $\delta^{238}U_{auth}$ for only limited U enrichments (Cole et al., 2020) but with a very low U-abundance weighted average $\Delta^{238}U_{anox}$ of ~0.1‰.

3.2. *Sapropels*

3.2.1. *Interpretative framework*

Quaternary aged Mediterranean sapropels are used to further investigate $\delta^{238}U_{auth}$ systematics. Sapropels are organic-rich intervals from the Mediterranean where anoxia is thought to have been driven by a combination of stratification and enhanced productivity linked to precession modulation of monsoon dynamics (Rohling et al., 2015). Sapropels have the advantage of recording time-averaged conditions over several kyrs, rather than the snapshot offered by modern sediments. Moreover, they represent the largest oxic-anoxic transitions for the Quaternary where depositional conditions are well understood and good age models are available (Grant et al., 2016) to calculate organic carbon and metal accumulation rates (see section 3.2.3). The sapropel data presented here come from two localities in the Eastern Mediterranean (Site 967 at ~2100 m depth, and Site 46PE406-E1 at ~1700 m depth)

and cover several sapropel events (S1 to S9 deposited during the last 250 kyr) that systematically capture different degrees of deoxygenation, H_2S concentrations and bottom-water renewal times (Rohling et al., 2002; Rohling et al., 2015; Andersen et al., 2018; Andersen et al., 2020; Hennekam et al., 2020; Clarkson et al., 2021a; Sweere et al., 2021; Chiu et al., 2022). By using multiple sapropels from two nearby cores, the effect of secondary environmental variabilities on $\delta^{238}U_{auth}$ should be minimised, allowing for a more direct comparison of U reduction mechanisms under different redox regimes.

Updated MoEF–UEF trends (Fig. 6) and $\delta^{98}Mo_{auth}$ data (Fig. 7) are used to qualitatively define the degree of euxinia for these samples (This study; Andersen et al., 2018; Andersen et al., 2020; Sweere et al., 2021; Chiu et al., 2022). Sapropels from Site 967 tend to show larger Mo and U enrichments compared to Site 64PE406-E1 (Fig. 6), indicative of more reducing conditions as a consequence of lower ventilation rates at the deeper Site 967 (De Lange et al., 2008; Chiu et al., 2022). The most well developed sapropel is S5, followed by S7, where both are thought to have been strongly euxinic during peak sapropel development with large Mo and U enrichments (Fig. 6). At the peak of these two events, water-column H_2S_{total} concentrations were greater than the thiomolybdate switch point of 100 μmol/mol (Neubert et al., 2008) resulting in largely quantitative Mo sulfidation and $\delta^{98}Mo_{auth}$ (Sweere et al., 2021; Chiu et al., 2022) similar to modern seawater (~2.3‰; Archer and Vance, 2008). By contrast, S3, 4, 6, 8 and 9 were less well developed and moderately euxinic with lower Mo and U enrichments (Fig. 6) and a broad range of $\delta^{98}Mo_{auth}$ values below seawater values (Sweere et al., 2021). Sapropel S1 is the most poorly developed sapropel event and only weakly euxinic at peak conditions, with low MoEFs and UEFs, and $\delta^{98}Mo_{auth}$ are distinctly lower than the other sapropel events (This study; Andersen et al., 2020). For S1, geochemical evidence demonstrates enhanced ventilation during the event and Site 64PE406-E1 was strongly affected by post-depositional oxidation (i.e. "burndown") and loss of redox-sensitive trace metals and organic carbon (Fig. 6; De Rijk et al., 1999; Rohling et al., 2015; Clarkson et al., 2021a). In the upper sapropel samples from S1, Mn-cycling may be important for Mo systematics (Reitz et al., 2007), leading to a steep trajectory in MoEF–UEF space (Fig. 6). But there is no clear evidence of Mn-cycling affecting $\delta^{238}U_{auth}$ systematics that are dominated by reduction in these samples (Clarkson et al., 2021a). Such MoEF–UEF trends would also be consistent with oxidative loss of U and Mo, and low $\delta^{98}Mo_{auth}$ (Fig. 7) can be explained by partial sulfidation. S1 samples from Site 967, and from the onset of the sapropel at Site 64PE406-E1, do not show these complications (Andersen et al., 2020; Clarkson et al., 2021a). Other sapropels only show minor disturbance or complete preservation (Hennekam et al., 2020).

3.2.2. *Sapropel $\delta^{238}U_{auth}$ and $[U_{auth}]$*

For S5, there is a general positive correlation of $\delta^{238}U_{auth}$ and $[U_{auth}]$ at lower U enrichments (Fig. 3b), which are consistently below the diffusion-limited threshold value of +0.2‰. Like the Black Sea, $\delta^{238}U_{auth}$ decreases at $[U_{auth}] > \sim 10$ ppm. This trend is thought to signify bottom water U depletion due to long deep-water renewal times ($\sim 1030^{+820}_{-520}$ yrs) compared to today (~100 yrs), assuming a constant $\Delta^{238}U_{anox}$ of +0.6‰ throughout the sapropel event (Andersen et al., 2018; Chiu et al., 2022). These lower $\delta^{238}U_{auth}$ could also reflect a decrease in $\Delta^{238}U_{anox}$ due to more quantitative pore water U reduction (Lau et al., 2020) supported by MoEF/UEF ratios similar to modern seawater (Fig. 6).

For S7, $\delta^{238}U_{auth}$ reaches higher values up to +0.4‰ and more limited $[U_{auth}]$ compared to S5. The less reducing sapropels (S1, 3, 4, 6, 8, 9) tend toward higher $\delta^{238}U_{auth}$ at lower $[U_{auth}]$, with the highest $\delta^{238}U_{auth}$ value seen in S1 (Fig. 3b; Andersen et al., 2020; Clarkson et al., 2021a). The differences in U isotope systematics between the sapropels are summarized in Fig. 4 and Table 2. Whilst the U-abundance weighted average $\Delta^{238}U_{anox}$ are similar between the sapropels, the less reducing sapropels tend to have higher $\Delta^{238}U_{anox}$ than S5, and above the diffusion-limited threshold. The U-abundance weighted average $\Delta^{238}U_{anox}$ of the entire sapropel dataset is slightly below the diffusion-limited threshold at +0.53‰, and similar to modern euxinic basins, but higher than the global marine value of +0.4‰.

3.2.3. *Isotope systematics with organic carbon and metal accumulation rates*

For Site 46PE406-E1, we further examine $\delta^{238}U_{auth}$ combined with

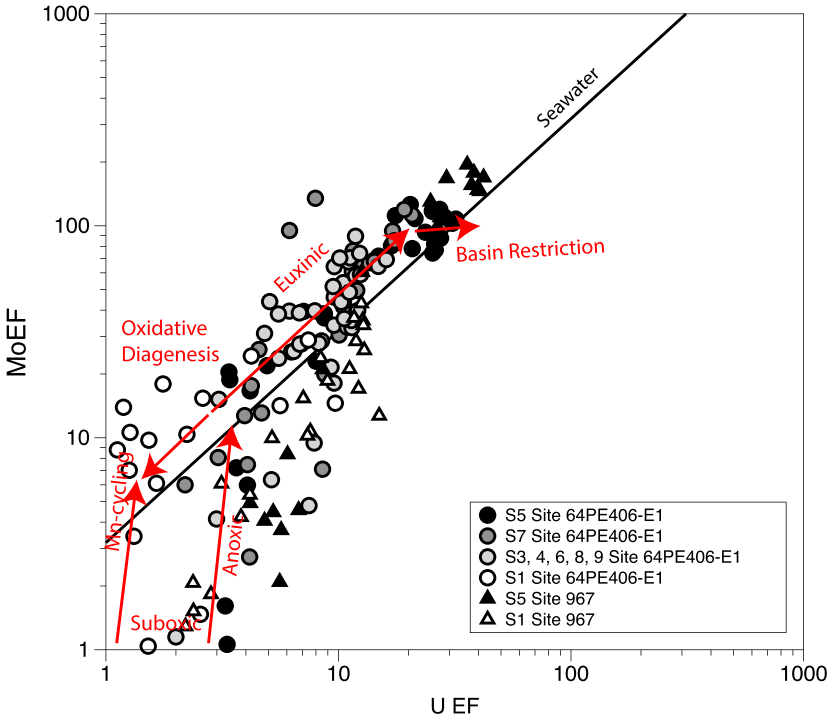

Fig. 6. Mo and U enrichment factor (EF) framework used to help constrain interpretations from $\delta^{98}Mo$ in sapropel data. Interpretative trajectories after Algeo and Tribovillard (2009). Most samples show a consistent relationship that is close to the seawater trend, suggesting variable enrichments under euxinic conditions. Some samples plot with higher MoEF/UEF which capture redox variation associated with the onset or end of sapropels. Some S1 samples show a steeper MoEF–UEF relationship that may indicate Mo enrichment from Mn cycling and/or U loss during post-depositional oxidative diagenesis. Note that data from Site 967 are recalculated after Andersen et al. (2018, 2020) using local detrital estimates from Site 64PE406-E1 (Clarkson et al., 2021a; Chiu et al., 2022).

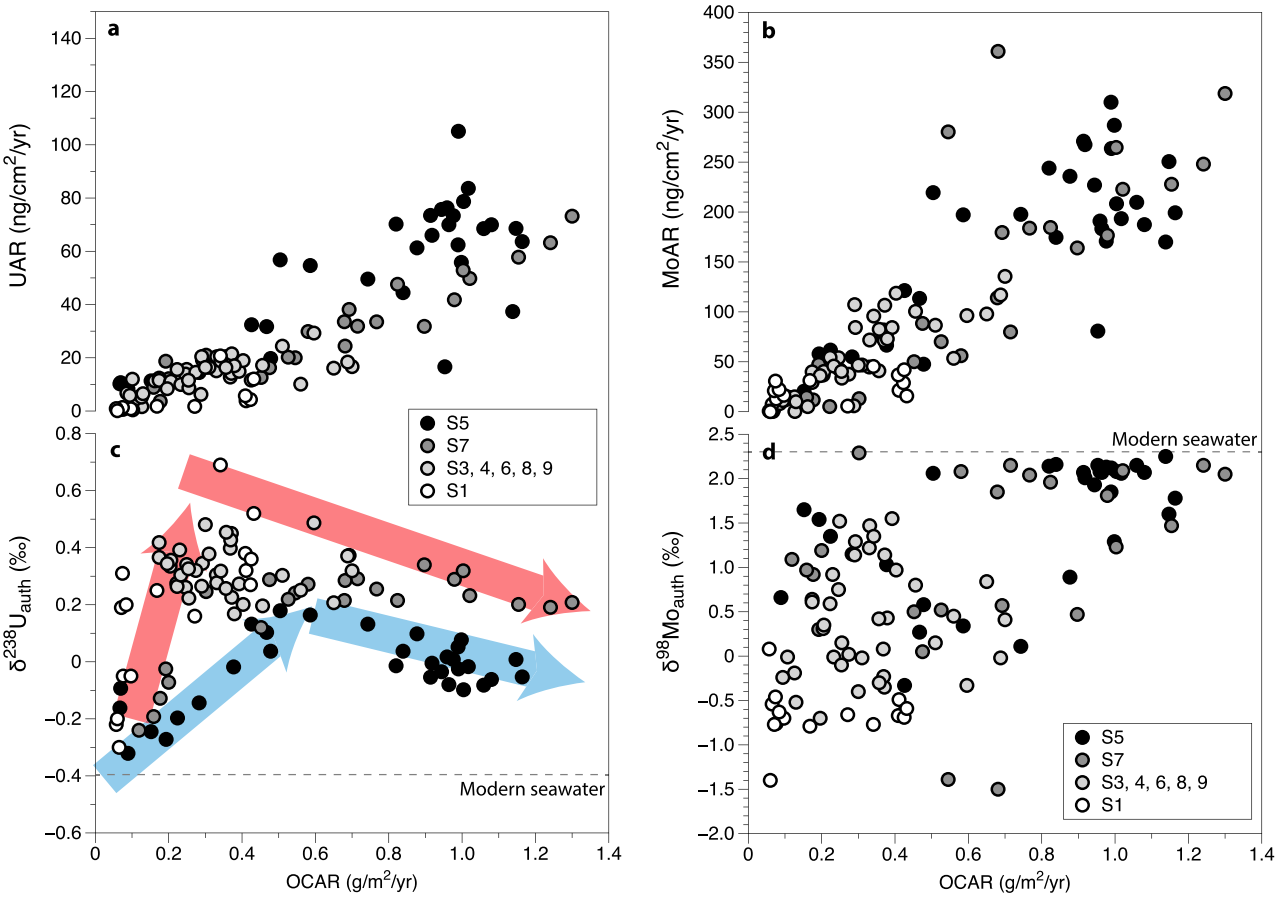

Fig. 7. Sapropel U and Mo systematics as a function of organic carbon accumulation rates (OCAR). a and b illustrate the positive correlation between U and Mo accumulation rates (UAR, MoAR) with increasing OCAR. **c** $\delta^{238}U_{auth}$ shows the highest values at low – intermediate OCAR associated with lower UAR in the weakest sapropel events. These samples also show $\delta^{98}Mo$ evidence for lower H_2S concentrations in **d.** Higher MoAR tend to occur at higher OCAR and record seawater $\delta^{98}Mo$ due to quantitative Mo removal. Weaker sapropel events tend toward $\delta^{238}U_{auth} = +0.2‰$ with increasing OCAR and UAR (red arrow) reflecting the mixing of diffusion-limited and non-diffusion-limited U(IV). Sapropel S5 (blue arrows) shows a dominance of diffusion-limited U(IV) throughout, and the effects of bottom water U depletion or quantitative U removal at higher OCAR. (For interpretation of the references to colour in this figure legend, the reader is referred to the web version of this article.)

Table 2
Summary statistics for reducing sediment compilation.

Classification		U-abundance weighted average $\Delta^{238}U_{anox}$ (‰)
Modern	Hypoxic	+ 0.53
	Black Sea Chemocline	+ 0.80
	Black Sea Unit II	+ 0.74
	Euxinic Basins	+ 0.51
	Upwelling	+ 0.24
	Ferruginous lakes	+ 0.14
	Global Marine Reducing	+ 0.40
Sapropel	S1	+ 0.81
	S3, 4, 6, 8, 9	+ 0.63
	S7	+ 0.64
	S5	+ 0.40
	All Sapropel	+ 0.53

$\delta^{98}Mo_{auth}$ from the same samples (This study; Andersen et al., 2018; Andersen et al., 2020; Sweere et al., 2021; Chiu et al., 2022), in the context of organic carbon and authigenic metal accumulation rates (Fig. 7; OCAR, UAR, MoAR). Whilst OCAR reflects both productivity and preservation, it serves as an independent proxy for the severity of local redox conditions and allows comparison to reaction transport model predictions (Lau et al., 2020; see section 4.1). Moreover, examining U and Mo systematics using accumulation rates helps normalize for variable dilution effects due to admixtures of carbonate, siliciclastic and organic carbon components. Since most studies cannot accurately estimate mass accumulation rates, we also show the equivalent authigenic concentration and isotope data as a function of TOC in Fig. S3 but focus on AR here. UAR and MoAR are positively correlated with OCAR across all sapropels (Fig. 7a, b) and similar to those reported for the Black Sea (UAR = ~60–200 ng/cm^2/yr, Dunk et al., 2002; MoAR = 196 ng/cm^2/yr, Algeo & Lyons 2006; OCAR = ~0.69–2.09 g/m^2/yr, Calvert et al., 1998). Note that some samples may show lower apparent OCAR and metal AR due to post-depositional oxidative diagenesis, but this is likely restricted to S1 samples that show clear evidence for U loss (Clarkson et al., 2021a) and are identifiable by very low OCAR in Fig. 7c. Variability in sapropel UAR and MoAR might reflect the importance of decreased bottom water ventilation and limited O_2 supply on local redox conditions, but the role of PNU delivery for U supply cannot be discounted.

The relationship of $\delta^{238}U_{auth}$ with OCAR is less straightforward but similar to the relationships of $\delta^{238}U_{auth}$ with $[U]_{auth}$ (Fig. 3). The $\delta^{238}U_{auth}$ of the strongly euxinic sapropel S5 shows an increase with OCAR but remains below the diffusion-limited threshold of +0.2‰ (Andersen et al., 2014). At OCAR > ~0.6 g/m^2/yr, $\delta^{238}U_{auth}$ for S5 decreases, corresponding to samples with higher $[U_{auth}]$ and UAR. By contrast, the higher $\delta^{238}U_{auth}$ of the weaker sapropels (S1, 3, 4, 6, 9) are associated with low–intermediate OCAR (0.1–0.7 g/m^2/yr). The non-S5

sapropels collectively show a decrease in maximum $\delta^{238}U_{auth}$ and variability with increasing OCAR, down to the diffusion-limited value of +0.2‰.

Sapropels S5 and S7 tend to show higher MoAR at higher OCAR. Some of these samples show high $\delta^{98}Mo_{auth}$ close to modern seawater values (~2.3‰; Archer and Vance, 2008), indicating strongly euxinic conditions (Andersen et al., 2018; Chiu et al., 2022). Samples with lower MoAR and $\delta^{98}Mo_{auth}$ record intermediate conditions during the onset or termination of the sapropel events. Some samples with lower MoAR and OCAR also record seawater-like $\delta^{98}Mo_{auth}$ values. These samples likely reflect Mo removal within sulfidic porewaters, but beneath a more oxygenated water column, with more limited Mo enrichment (Scott and Lyons, 2012). Alternatively, short-lived bottom water euxinic episodes could explain these data. The less developed sapropels (S1, 3, 4, 6, 8, 9) record a wide range of $\delta^{98}Mo_{auth}$ values across low–intermediate OCAR (<0.7 g/m^2/yr), but are always lower than modern seawater (Fig. 7) reflecting partial sulfidation and non-quantitative Mo removal (Sweere et al., 2021). Samples from S1 (this study), with OCAR <0.5 g/m^2/yr, have generally much lower $\delta^{98}Mo_{auth}$ compared to the other sapropels (−1.4 to +0.1‰).

3.3. U and Mo isotope covariation

The sapropel samples from Site 46PE406-E1 show covarying Mo and U isotope systematics according to OCAR and hence local redox conditions. These behaviours create distinct trajectories when examined within $\delta^{98}Mo_{auth}$–$\delta^{238}U_{auth}$ space (Fig. 8), trends that are shared by modern samples. In short, strongly euxinic samples (Black Sea basin, Cariaco and the better developed sapropels) tend to show intermediate or lower $\delta^{238}U_{auth}$ with higher $\delta^{98}Mo_{auth}$. The Black Sea basin and S5 samples tend toward the lowest $\delta^{238}U_{auth}$ values whilst less developed sapropels are closer to +0.2‰. By contrast, Black Sea chemocline and the most poorly developed sapropels tend to show the highest $\delta^{238}U_{auth}$ with lower $\delta^{98}Mo_{auth}$.

4. Discussion

4.1. Environmental controls on high $\Delta^{238}U_{anox}$

Extremely low Neoproterozoic $\delta^{238}U_{sw}$ requires a U-abundance weighted average $\Delta^{238}U_{anox}$ of at least +0.9‰, higher than the diffusion-limited threshold. Assuming that large amounts of U burial also expressed lower isotope enrichments, and given that non-reducing U sinks also existed, it is likely that a high proportion of U sinks had even higher $\Delta^{238}U_{anox}$ values, closer to the full theoretical enrichment factor of ~+1.2‰. Such high $\delta^{238}U_{auth}$ values are poorly represented in published modern datasets. But the above re-examination, in particular using UCC or local $U/Al_{detrital}$ for authigenic correction, and together with the trends identified in sapropel samples, shows that these high $\Delta^{238}U_{anox}$ values tend to be associated with i) hypoxic settings; ii) anoxic settings with lower water-column H_2S concentrations; iii) the onset of weaker sapropel events, and iv) low–intermediate OCAR and UAR. The modern and sapropel data compilation demonstrates that the only anoxic environments to record a U-abundance weighted average $\Delta^{238}U_{anox}$ above +0.6‰ are modern chemocline sediments from the Black Sea and weakly euxinic sapropels (Fig. 4).

Very high $\Delta^{238}U_{anox}$ (above +0.6‰) are thought to be an expression of either i) partial U removal under a diffusion-limited regime in hypoxic settings, which leads to correspondingly low U enrichments, or ii) non-diffusion-limited U reduction in anoxic settings (Andersen et al., 2014; Andersen et al., 2017). The high $\Delta^{238}U_{anox}$ associated with partial U reduction in hypoxic settings are caused by a slower rate of U depletion in porewaters that effectively decreases diffusion-limitation to the reduction site (Fig. 9; Andersen et al., 2014). Previous work also highlights the higher permeability associated with coarser grainsizes to explain the very high $\Delta^{238}U_{anox}$ data from Toulon Bay (Dang et al., 2018), but the wider applicability of this control remains unknown. Conversely, hypoxic samples with very low $\Delta^{238}U_{anox}$ likely reflect more quantitative U reduction in porewaters due to even greater oxygen

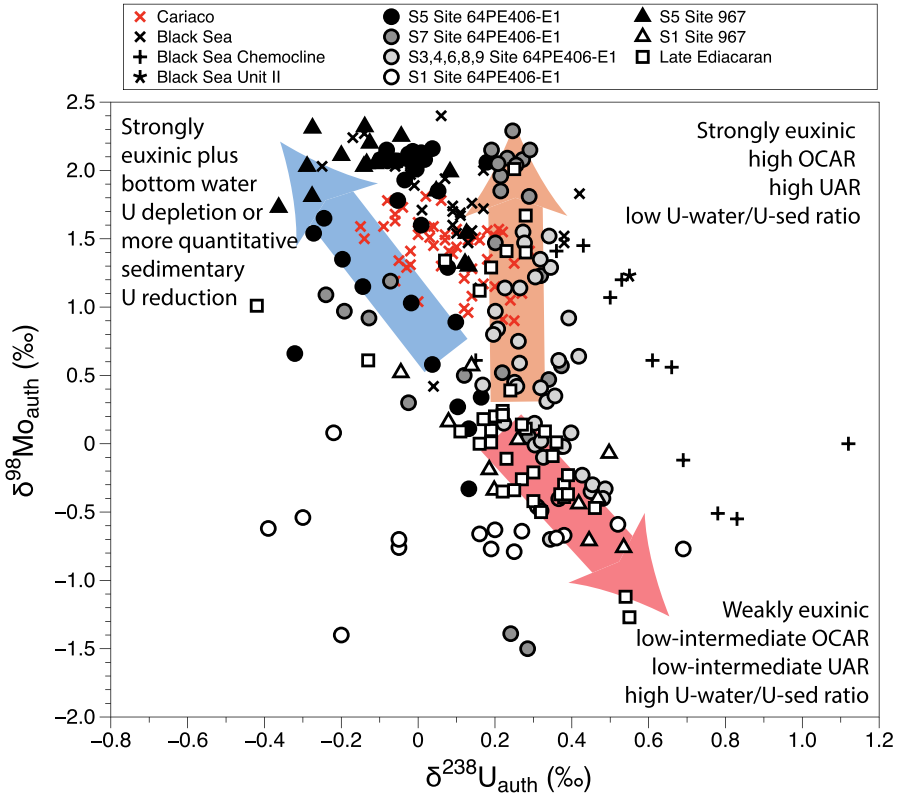

Fig. 8. Comparison of U and Mo isotope systematics for anoxic sediments. Data for modern euxinic settings (Brüske et al., 2020b) and the Mediterranean sapropels (This study; Sweere et al., 2021; Chiu et al., 2022) show similar trajectories that separate according to strength of euxinia. High $\delta^{238}U_{auth}$ have distinctly lower $\delta^{98}Mo_{auth}$ values, suggestive of partial Mo sulfidation and only weakly euxinic conditions whilst samples that record $\delta^{98}Mo_{auth}$ that are closer to seawater tend to show lower $\delta^{238}U_{auth}$ values. Samples that show evidence of basin restriction and bottom water U depletion show the lowest $\delta^{238}U_{auth}$ values but $\delta^{98}Mo_{auth}$ closer to modern seawater. Late Ediacaran shales (open squares; Kendall et al., 2015) also fit these trends.

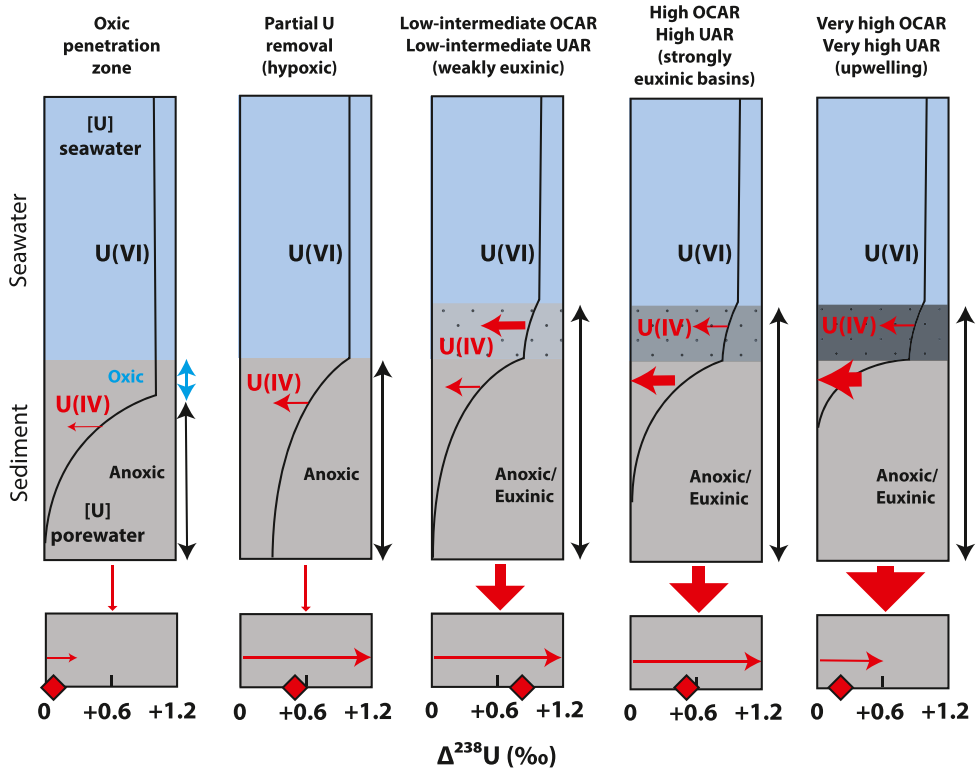

Fig. 9. Interpretative framework of controls in the expression of $\Delta^{238}U_{anox}$. Schematic model modified from Andersen et al. (2014, 2017) illustrating the net result of diffusion-limitation on U isotope fractionation and U flux for different settings. Upper panel illustrates the sedimentary redox environment and the impact on dissolved U concentrations of seawater and porewaters (black line). For scenarios that involve U reduction within an organic floc the ratio of sedimentary U(IV) to water column U(IV) varies depending on total UAR and OCAR. Dotted shading represent organic-rich floccule at the sediment water interface, and grey shading is the underlying sediment pile. Vertical red arrows connecting upper and lower panels are scaled for relative U flux. Lower panel shows the range of $\Delta^{238}U_{anox}$ observed in modern and recent sediments (horizontal red arrows) and the U-abundance weighted average (red diamonds) identified from anoxic sediments in this study. The average $\Delta^{238}U_{anox}$ for oxic sediments is taken as the global average oxic sink (Andersen et al., 2017). (For interpretation of the references to colour in this figure legend, the reader is referred to the web version of this article.)

penetration (Andersen et al., 2014; Andersen et al., 2016). Given the tendency for reduction mechanisms that result in very high or very low $\Delta^{238}U_{anox}$, the U-abundance weighted average for hypoxic sinks is +0.5‰. Note that this is a higher $\Delta^{238}U_{anox}$ than typically assigned to hypoxic settings (Andersen et al., 2017) and is driven largely by inclusion of the Toulon Bay samples (Dang et al., 2018). Further work is required to better characterise the importance of hypoxic sites for the global U isotope mass balance.

For fully anoxic environments, the environmental control on the prevalence of non-diffusion-limited U reduction is less well understood, with hypotheses focusing on reduction directly at or above the sediment-water interface. In this context, higher $\Delta^{238}U_{anox}$ could signify U reduction within a highly permeable organic floc layer (Andersen et al., 2017; Andersen et al., 2020; Cheng et al., 2020). Water column U reduction has also been proposed to remove diffusion-limitation controls (Cheng et al., 2020; Lau et al., 2020; Wei et al., 2021; Zhang et al., 2022) although water column reduction is not clearly evident in the Black Sea water column U concentration and isotope profiles (Rolison et al., 2017). Others have suggested that U reduction occurs on sinking organic matter and can be delivered to the sediment as PNU (Zheng et al., 2002; Scholz et al., 2011; Bruggmann et al., 2021; He et al., 2021) and could plausibly remove diffusion-limitation controls during U reduction.

Whilst requiring less diffusion-limitation, likely linked to organic carbon delivery, high organic carbon accumulation is not the defining characteristic of higher $\Delta^{238}U_{anox}$ (Andersen et al., 2020). This is clearly demonstrated in the sapropel compilation where higher $\delta^{238}U_{auth}$ are seen at low–intermediate OCAR (0.2–0.7 g/m^2/yr; Fig. 7), equivalent to ~2–5 wt% TOC (Fig, S3). This result is predicted by reaction transport modelling due to the mixing of U(IV) from different reduction regimes (Lau et al., 2020). One hypothetical U(IV) pool is reduced in the water column, as PNU or above the sediment in an organic floc ($\Delta^{238}U_{anox}$ > +0.6‰), whilst the second U(IV) pool accumulates in the sediment pile due to sediment reduction under a diffusion-limited regime ($\Delta^{238}U_{anox}$ < +0.6‰). Higher OCAR corresponds to higher UAR with a greater contribution of pore-water reduced U(IV) to the sediment mass balance relative to that supplied from the non-diffusion-limited regime. By contrast, at lower OCAR, less sedimentary U accumulation means the U (IV) pool with $\Delta^{238}U_{anox}$ > +0.6‰ dominates the mass balance (Fig. 9). This mixing behaviour likely explains the non-S5 sapropel data, where $\delta^{238}U_{auth}$ is higher at lower OCAR and decreases with increasing OCAR (Fig. 7), eventually reaching +0.2‰ ($\Delta^{238}U_{anox}$ = +0.6‰). The relatively constant UAR/OCAR of non-S5 samples (Fig. 7a) implies that the high $\delta^{238}U_{auth}$ values are not a function of increased particulate U delivery alone but is likely due to the decreased *relative* contribution of sedimentary authigenic U at low total UAR under weakly euxinic conditions. Similarly, the Black Sea chemocline samples have intermediate OCAR (0.69 g/m^2/kyr; Calvert et al., 1991), low [U_{auth}], high $\delta^{238}U_{auth}$ and low δ^{98}Mo (Figs. 7 & 8; Rolison et al., 2017; Brüske et al., 2020b), corresponding to modern water column [H_2S_{total}] <100 μmol/mol (Rolison et al., 2017) and porewater [H_2S_{total}] <500 μmol/mol (at 2 cm core depth; Barnes and Cochran, 1991).

Experimental studies suggest that larger $\Delta^{238}U_{anox}$ are expected at lower rates of U reduction (Brown et al., 2018) which would also be consistent with the trends seen in the sapropel and Black Sea chemocline datasets if U reduction rates scale with sulfate reduction rates and hence H_2S concentrations (Barnes and Cochran, 1993). The reaction transport model framework (Lau et al., 2020) further identifies that high $\Delta^{238}U_{anox}$ would be expected under conditions with a high proportion of non-diffusion-limited U(IV) but at high sedimentation rates. Rapid burial effectively decreases the sediment residence time, transporting the sediment package deeper than can be resupplied by diffusion, thus limiting pore-water U reduction. For the sapropels, however, sedimentation rates alone cannot explain high $\delta^{238}U_{auth}$ (Fig. S2).

The variable behaviour of $\delta^{238}U_{auth}$ between the different sapropels, and in the modern dataset, suggest that high $\delta^{238}U_{auth}$ might be a common feature of anoxic sediments. But, following the reactive transport model framework (Lau et al., 2020), sustained U accumulation appears to effectively mask the contribution from non-diffusion-limited U reduction in most anoxic settings. This is consistent with the

observation that the highest sapropel $\delta^{238}U_{auth}$ values occur at the onset of S1 and, specifically, at the shallower, better ventilated locality (De Rijk et al., 1999; Rohling et al., 2002; Andersen et al., 2020; Clarkson et al., 2021a). The abruptness of sapropel onset could also be important for dictating the U reduction regime for S1 (Andersen et al., 2020). A similar scenario might be applicable for the Black Sea Unit II, which represents the first establishment of anoxic conditions in the basin. More generally, PNU is thought to account for a large contribution of U in the Peru Margin sediments (up to 36% for anoxic sediments), with high inferred $\delta^{238}U_{auth}$ of $+0.17 \pm 0.63$‰, but total sediment $\delta^{238}U_{auth} < +0.2$‰ (Bruggmann et al., 2021). In Namibia, pore-water $\delta^{238}U > +0.2$‰ imply oxidative U release from a high $\delta^{238}U_{auth}$ source, but again sediment $\delta^{238}U_{auth}$ are consistently below the diffusion threshold (He et al., 2021). Identifying the wider role of PNU delivery is further potentially complicated by the adsorption of isotopically light U as particles settle through the water column that can dominate bulk sediment $\delta^{238}U_{auth}$ in rare cases (Holmden et al., 2015; Hinojosa et al., 2016). Such an increased supply of isotopically light U adsorbed to organic matter could be an additional contributor to the observed trends in the sapropel data, but no attempt has yet been made to quantify such contributions in reducing settings. Moreover, this model would still require a dominant non-diffusion-limited U(IV) pool at lower OCAR, thus not affecting the wider implications of this study.

The hypothesised importance of relatively low UAR for high $\Delta^{238}U_{anox}$ was previously suggested to explain the Black Sea Unit II samples (Andersen et al., 2014), but has since not been widely adopted as part of the modern framework for the dominant controls of U isotope fractionation in sediments. The data presented here systematically illustrate the control of UAR on the expression of $\Delta^{238}U_{anox}$, and based on the above discussion, we suggest a modification of previous frameworks (Andersen et al., 2014; Andersen et al., 2017). This updated framework (Fig. 9) hypothesises the presence of a non-diffusion-limited U(IV) pool for the majority of anoxic sites, but where the expression of $\Delta^{238}U_{anox}$ in the sediment depends on the ratio of sediment to water column (including PNU and organic floc) derived U(IV), and hence UAR.

4.2. Implications for Neoproterozoic records

4.2.1. Redox instability

If the above observations can be extended to the Neoproterozoic, one mechanism to explain high $\Delta^{238}U_{anox}$ is through progressive oxygenation and redox instability, acting via either i) partial U reduction with less diffusion-limitation in hypoxic settings or ii) greater relative contributions of non-diffusion-limited U(IV) under temporally dynamic anoxic conditions. In contrast to previous interpretations of more 'intense' anoxia during the late Ediacaran (Wei et al., 2021), this revised framework is more consistent with previous studies using local redox proxies (Fig. 1). Indeed, local redox tracers identify a highly dynamic redox landscape with temporary incursions of predominantly low oxygen (manganous) or anoxic non-sulfidic (ferruginous) waters onto oxygenated shelf environments but with great spatial heterogeneity where phases of biotic turnover or change have not been established to be coincident with episodes of anoxia (Wood et al., 2015; Och et al., 2016; Tostevin et al., 2016; Bowyer et al., 2017; Wood et al., 2019). Globally, the predominantly anoxic post-Sturtian ocean saw frequent oceanic oxygenation events that likely became progressively stronger into the Phanerozoic with the gradual build-up of atmospheric and oceanic dissolved O_2 (Chen et al., 2015; Pogge von Strandmann et al., 2015; Sahoo et al., 2016; Lyons et al., 2021; Chen et al., 2022; Shi et al., 2022). Thus, the very low $\delta^{238}U_{sw}$ values of the late Ediacaran may reflect the global expansion of anoxia into more oxygenated shelf environments, but with low–intermediate U accumulation rates associated with highly dynamic, and overall, less-reducing conditions. The change in U isotope systematics could plausibly reflect a broader chemocline (i.e. less-stratified) or less stable conditions as the stratified anoxic ocean of the Paleo- and Mesoproterozoic gave way to more oxygenated conditions in the late Neoproterozoic. Far less is known about local redox dynamics in the Tonian, but the same interpretation of increased oxygenation could be relevant (Dang et al., 2022), rather than an increase in water column U reduction and higher productivity (Zhang et al., 2022). Indeed, the Tonian $\delta^{238}U_{carb}$ record shows two intervals of higher values (Zhang et al., 2022) and high $\Delta^{238}U_{anox}$ have been inferred in more oxygenated sediments throughout the Meso-Neoproterozoic (Dang et al., 2022).

The Neoproterozoic U isotope records may have been further affected by redox structure through the availability of dissolved U. After long periods of widespread anoxia the deep ocean would have been depleted in U (Lyons et al., 2014). Such stratification could potentially lead to a build-up of dissolved U in the oxic surface ocean. As a result, U reduction would then preferentially occur close to the chemocline, compared to deeper locations where U supply would be severely limited. Moreover, U reduction from a depleted U pool in the deep ocean would be expected to be more quantitative, resulting in smaller isotope fractionation. Thus, redox structure could bias the global $\delta^{238}U_{sw}$ record toward shallow water processes where redox conditions would be inherently more dynamic, preventing substantial sedimentary U reduction.

4.2.2. Euxinic transitions

The data presented here further identify that weakly euxinic water column conditions (i.e. $[H_2S_{total}] <100$ μmol/mol) can be important for very high $\Delta^{238}U_{anox}$. The same constraint is apparent in late Ediacaran shales from the Doushantou Formation (Kendall et al., 2015), which show a similar relationship in $\delta^{238}U_{auth}$–$\delta^{98}Mo_{auth}$ space as the less developed sapropels and Black Sea chemocline samples (Fig. 8); higher $\delta^{238}U_{auth}$ associated with lower $\delta^{98}Mo_{auth}$. More broadly, similar $\delta^{238}U_{auth}$–$\delta^{98}Mo_{auth}$ relationships are seen in shales from the Great Oxidation Event, Early Cambrian and Devonian (Asael et al., 2013; Andersen et al., 2020; Cheng et al., 2020; Kendall et al., 2020) suggesting that this control is widely applicable.

The influence of such weakly euxinic conditions on U isotope systematics could be a feature of major transitions in ocean chemistry through the Neoproterozoic. Specifically, a retraction of mid-depth euxinia and dominance of ferruginous conditions is documented around the Meso-Neoproterozoic boundary (Fig. 1; between 1.1 and 0.8 Ga), potentially driven by an influx of Fe from weathering and the breakup of Rodinia (Guilbaud et al., 2015). If this transition phase were associated with weakly euxinic conditions, it could plausibly explain the very low early Tonian $\delta^{238}U_{sw}$. Ferruginous conditions remained dominant through the Neoproterozoic to the Cambrian (Canfield et al., 2008; Sperling et al., 2015), with mid-depth euxinia limited to the Yangtze Block, South China, from ~635 Ma where it was highly intermittent and with strong local environmental controls (Li et al., 2010; Och et al., 2016; Bowyer et al., 2017). Sulfate concentrations increased in the late Neoproterozoic to Paleozoic, possibly driven by a pulse of evaporite weathering ~575 Ma and potentially causing the Shurum oxygenation event (Shields et al., 2019; Shi et al., 2022). But, sulfate concentrations likely decreased again toward the onset of the most extreme $\delta^{238}U_{carb}$ excursion in the Late Ediacaran at ~550 Ma (Shi et al., 2022). Thus, like the early Tonian, the late Ediacaran experienced major changes in the balance between iron and sulfate supply and removal, marking transitions between predominantly ferruginous and euxinic mid-depth conditions. These transitions were plausibly associated with weakly euxinic conditions that would explain the very high $\Delta^{238}U_{anox}$ and very low $\delta^{238}U_{sw}$ values.

Whilst providing a hypothesis for very low $\delta^{238}U_{sw}$ values, understanding the importance of longer-term changes in iron and sulfate availability for the U isotope record is challenging. Firstly, our understanding of U isotope fractionation in ferruginous sediments is extremely limited. Modern ferruginous lake sediments show a low U-abundance weighted average $\Delta^{238}U_{anox}$ (Fig. 4; Cole et al., 2020) but the range is large. It is also unclear how applicable these lake findings are to

ferruginous oceans, given the potential effects of U speciation on isotope fractionation (Chen et al., 2016). Moreover, higher $\Delta^{238}U_{anox}$ values (up to +0.6‰) have been inferred for Neoproterozoic ferruginous marine samples (Dang et al., 2022). Secondly, interpretation using current Proterozoic geochemical frameworks is limited by the ability to identify low levels of dissolved sulfide (see also Scott and Lyons, 2012). For example, Fe-speciation is widely used to separate euxinic and ferruginous depositional environments through this period (e.g. Li et al., 2010; Poulton and Canfield, 2011; Sperling et al., 2015; Och et al., 2016; Bowyer et al., 2017). But, in weakly euxinic sapropel events, large pyrite enrichments above the Fe-speciation threshold indicative of euxinia are not present (S1 & S7 and even after accounting for local detrital Fe-oxide enrichments; Matthews et al., 2017; Benkovitz et al., 2020). Thus, these conditions could easily be mistaken for ferruginous environments in the rock record. We suggest that distinct array trajectories in $\delta^{238}U_{auth}$–$\delta^{98}Mo_{auth}$ space might provide a better way to characterise subtle changes in euxinia (Fig. 8), albeit itself complicated by changes in global seawater isotope compositions. Finally, the tendency for samples with very high $\Delta^{238}U_{anox}$ to have lower [U_{auth}] makes it difficult to identify these samples using bulk measurements. We recommend that leaching approaches (Clarkson et al., 2021a; Dang et al., 2022) be used in order to avoid the uncertainties of detrital corrections for $\delta^{238}U_{auth}$ estimates.

4.3. Wider implications

4.3.1. Shale archives

The large degree of $\delta^{238}U_{auth}$ variability found in reducing settings, with strong environmental controls, have wider implications for the use of U isotopes as a quantitative global redox indicator. It is common to use anoxic shales as an archive to reconstruct $\delta^{238}U_{sw}$, for short term perturbation events such as the mid-Cretaceous Oceanic Anoxic Event 2 (OAE2; Montoya-Pino et al., 2010; McDonald et al., 2022), snapshots of pre-Cambrian conditions (Kendall et al., 2015) and for secular changes through Earth history such as the Eocene-Oligocene transition (Dickson et al., 2021). In all cases knowledge of $\Delta^{238}U_{anox}$ is critical to reconstruct global $\delta^{238}U_{sw}$, most often assuming the diffusion-limited value of +0.6‰. The compilation presented here demonstrates that there are clearly large uncertainties in this approach as anoxic sediments could show any $\Delta^{238}U_{anox}$ between 0 and + 1.2‰. These findings support previous work highlighting the importance of basin hydrography, organic carbon rain rate and sedimentation rate on $\Delta^{238}U_{anox}$ (Lau et al., 2020; Lau et al., 2022), adding the complexity of local sulfide levels and redox stability to the list of controls. Ultimately, these findings challenge the use of shale archives to reconstruct $\delta^{238}U_{sw}$.

It is obviously difficult to identify primary trends in $\delta^{238}U_{sw}$ through an anoxic sedimentary section if $\Delta^{238}U_{anox}$ varies substantially in a single locality. This may be clear for measurement intervals below the residence time of U (Dickson et al., 2021) but is also relevant to longer-term records (e.g. Kendall et al., 2015; Wei et al., 2018; Wei et al., 2020). Such environmentally controlled variation can potentially be identified using MoEF–UEF (Algeo and Tribovillard, 2009) and $\delta^{98}Mo$–$\delta^{238}U$ frameworks (Figs. 6 & 8), supported by Fe-speciation (e.g. Stockey et al., 2020; Dickson et al., 2021; but also see 4.2.2). In a recent case for OAE2, McDonald et al. (2022) suggest varying $\Delta^{238}U_{anox}$ through a section to explain differences in estimated $\delta^{238}U_{sw}$ from contemporary archives. Whilst this concept is likely closer to reality than applying a constant $\Delta^{238}U_{anox}$ (Montoya-Pino et al., 2010) they assume a positive correlation between TOC and $\Delta^{238}U_{anox}$, which is not supported by the compilations presented here. In fact, the opposite may be true. We urge for greater consideration of how $\Delta^{238}U_{anox}$ varies within a studied interval and call for larger error propagation to account for the variability in $\Delta^{238}U_{anox}$ in modern reducing sediments.

4.3.2. Carbonate archives and mass balance models

When using oxic carbonates as an archive for $\delta^{238}U_{sw}$, assumptions on the global U-abundance weighted average $\Delta^{238}U_{anox}$ are required to estimate the areal extent of seafloor anoxia using isotope mass balance models. Again, most studies have used the +0.6‰ but also test higher and lower scenarios. To date, only one study uses contemporary anoxic sediments to estimate $\Delta^{238}U_{anox}$, but from a single locality, and supported a $\Delta^{238}U_{anox}$ of ~ + 0.5‰ for mass balance modelling (Clarkson et al., 2018). The use of contemporary oxic carbonate and anoxic shale records in this manner is encouraged but will always be limited by the availability of the geological record. Moreover, anoxic settings of lower U burial rates but higher $\Delta^{238}U_{anox}$ may not be the obvious target for investigation but could have significant implications for global U burial depending, for example, on paleogeography, shelf hypsometry or chemocline structure. If the global distribution of ancient redox environments was similar to the modern (i.e. similar relative proportions of upwelling sites and restricted basins) the modern global U-abundance weighted average $\Delta^{238}U_{anox}$ of +0.4‰ could be used for mass balance models. If this assumption cannot be made (e.g. during times of global stratification or widespread epeiric seas), there will be greater uncertainty. Our findings therefore make the case for developing spatially resolved, process-based biogeochemical models that integrate U isotopes, to advance on simpler two-sink biogeochemical model approaches (Clarkson et al., 2018; Zhang et al., 2020b).

5. Conclusion

The most direct interpretation for very low Neoproterozoic $\delta^{238}U_{sw}$ is a relative increase in the burial flux of U(IV) formed under a non-diffusion-limited regime. How this translates into the global extent, location or intensity of reducing conditions is less clear. The compilation presented here demonstrates that very high $\Delta^{238}U_{anox}$ are consistently associated with less reducing environments, dynamic fluctuations in redox conditions and weak euxinia. All of these environments prevent high U accumulation rates via sedimentary reduction. With the revised interpretation of high $\Delta^{238}U_{anox}$ based on modern and sapropel samples, the late Ediacaran $\delta^{238}U_{sw}$ record is more consistent with the temporally dynamic redox history suggested by other biological and geochemical datasets (Tostevin and Mills, 2020). Alternatively, the very low $\delta^{238}U_{sw}$ inferred for the Tonian and Late Ediacaran could reflect weakly euxinic conditions during transition intervals between predominantly ferruginous and euxinic mid-depth waters (Canfield et al., 2008; Guilbaud et al., 2015; Shields et al., 2019; Shi et al., 2022). This study highlights that interpretation of $\delta^{238}U_{sw}$ as changes in the global extent of anoxia are complicated by changes in U reduction regime, which appear to have important spatial and chemical controls. Thus, lower $\delta^{238}U_{sw}$ cannot always be interpreted as more widespread anoxia.

Declaration of Competing Interest

The authors declare that they have no known competing financial interests or personal relationships that could have appeared to influence the work reported in this paper.

Data availability

All data presented in this paper are available in the Supplementary Information

Acknowledgements

RW and FB acknowledge NERC Project NE/T008458/1. RW acknowledges support from an ETH visiting professorship. TCS has received funding from the European Union's Horizon 2020 research and innovation programme under the Marie Skłodowska-Curie grant agreement No. 834236. We thank the crew of the R/V Pelagia for obtaining the 64PE406-E1 core material during the first Netherlands Earth System Science Centre (NESSC) cruise. The NESSC program is carried out under financial support by the Dutch Ministry of Education,

Culture and Science (OCW; Grant 024.002.001). Thanks to Derek Vance, Morten Andersen, Eva Stüeken, Brian Kendall and an anonymous reviewer for comments.

Appendix A. Supplementary data

Supplementary data to this article can be found online at https://doi.org/10.1016/j.earscirev.2022.104306.

References

Abe, M., Suzuki, T., Fujii, Y., Hada, M., Hirao, K., 2008. An ab initio molecular orbital study of the nuclear volume effects in uranium isotope fractionations. J. Chem. Phys. 129 (16), 164309.

Abshire, M.L., Romaniello, S.J., Kuzminov, A.M., Cofrancesco, J., Severmann, S., Riedinger, N., 2020. Uranium isotopes as a proxy for primary depositional redox conditions in organic-rich marine systems. Earth Planet. Sci. Lett. 529, 115878.

Algeo, T.J., Tribovillard, N., 2009. Environmental analysis of paleoceanographic systems based on molybdenum–uranium covariation. Chem. Geol. 268 (3–4), 211–225.

Andersen, M., Matthews, A., Bar-Matthews, M., Vance, D., 2020. Rapid onset of ocean anoxia shown by high U and low Mo isotope compositions of sapropel S1. Geochem. Perspect. Lett. 15, 10–14.

Andersen, M., Romaniello, S., Vance, D., Little, S., Herdman, R., Lyons, T., 2014. A modern framework for the interpretation of 238U/235U in studies of ancient ocean redox. Earth Planet. Sci. Lett. 400, 184–194.

Andersen, M., Stirling, C.H., Weyer, S., 2017. Uranium isotope fractionation. Rev. Mineral. Geochem. 82 (1), 799–850.

Andersen, M., Vance, D., Morford, J., Bura-Nakić, E., Breitenbach, S., Och, L., 2016. Closing in on the marine 238U/235U budget. Chem. Geol. 420, 11–22.

Andersen, M.B., Elliott, T., Freymuth, H., Sims, K.W., Niu, Y., Kelley, K.A., 2015. The terrestrial uranium isotope cycle. Nature 517 (7534), 356–359.

Andersen, M.B., Matthews, A., Vance, D., Bar-Matthews, M., Archer, C., de Souza, G., 2018. A 10-fold decline in the deep Eastern Mediterranean thermohaline overturning circulation during the last interglacial period. Earth Planet. Sci. Lett. 503, 58–67.

Archer, C., Vance, D., 2008. The isotopic signature of the global riverine molybdenum flux and anoxia in the ancient oceans. Nat. Geosci. 1 (9), 597.

Asael, D., Tissot, F.L., Reinhard, C.T., Rouxel, O., Dauphas, N., Lyons, T.W., Ponzevera, E., Liorzou, C., Chéron, S., 2013. Coupled molybdenum, iron and uranium stable isotopes as oceanic paleoredox proxies during the Paleoproterozoic Shunga Event. Chem. Geol. 362, 193–210.

Azmy, K., Kendall, B., Brand, U., Stouge, S., Gordon, G.W., 2015. Redox conditions across the Cambrian-Ordovician boundary: Elemental and isotopic signatures retained in the GSSP carbonates. Palaeogeogr. Palaeoclimatol. Palaeoecol. 440, 440–454.

Barnes, C.E., Cochran, J.K., 1991. Geochemistry of uranium in Black Sea sediments. Deep Sea Research Part a. Oceanogr. Res. Pap. 38, S1237–S1254.

Barnes, C.E., Cochran, J.K., 1993. Uranium geochemistry in estuarine sediments: controls on removal and release processes. Geochim. Cosmochim. Acta 57 (3), 555–569.

Bartlett, R., Elrick, M., Wheeley, J.R., Polyak, V., Desrochers, A., Asmerom, Y., 2018. Abrupt global-ocean anoxia during the late Ordovician–early Silurian detected using uranium isotopes of marine carbonates. Proc. Natl. Acad. Sci. 115 (23), 5896–5901.

Basu, A., Sanford, R.A., Johnson, T.M., Lundstrom, C.C., Löffler, F.E., 2014. Uranium isotopic fractionation factors during U(VI) reduction by bacterial isolates. Geochim. Cosmochim. Acta 136, 100–113.

Benkovitz, A., Matthews, A., Teutsch, N., Poulton, S.W., Bar-Matthews, M., Almogi-Labin, A., 2020. Tracing water column euxinia in Eastern Mediterranean Sapropels S5 and S7. Chem. Geol. 545, 119627.

Bowyer, F., Wood, R., Poulton, S., 2017. Controls on the evolution of Ediacaran metazoan ecosystems: a redox perspective. Geobiology 15 (4), 516–551.

Bowyer, F.T., Zhuravlev, A.Y., Wood, R., Shields, G.A., Zhou, Y., Curtis, A., Poulton, S. W., Condon, D.J., Yang, C., Zhu, M., 2022. Calibrating the temporal and spatial dynamics of the Ediacaran-Cambrian radiation of animals. Earth Sci. Rev. 225, 103913.

Brennecka, G.A., Herrmann, A.D., Algeo, T.J., Anbar, A.D., 2011. Rapid expansion of oceanic anoxia immediately before the end-Permian mass extinction. Proc. Natl. Acad. Sci. USA 108 (43), 17631–17634. https://doi.org/10.1073/pnas.1106039108.

Brennecka, G.A., Wasylenki, L.E., Bargar, J.R., Weyer, S., Anbar, A.D., 2011b. Uranium Isotope Fractionation during Adsorption to Mn-Oxyhydroxides. Environ. Sci. Technol. 45 (4), 1370–1375. https://doi.org/10.1021/es103061v.

Brown, S.T., Basu, A., Ding, X., Christensen, J.N., DePaolo, D.J., 2018. Uranium isotope fractionation by abiotic reductive precipitation. Proc. Natl. Acad. Sci. 115 (35), 8688.

Bruggmann, S., Gilleaudeau, G.J., Romaniello, S.J., Severmann, S., Canfield, D.E., Anbar, A.D., Scholz, F., Frei, R., 2021. Uranium isotope cycling on the highly productive peruvian margin. Chem. Geol. 120705 https://doi.org/10.1016/j.chemgeo.2021.120705.

Brüske, A., Martin, A., Rammensee, P., Eroglu, S., Lazarov, M., Albut, G., Schuth, S., Aulbach, S., Schoenberg, R., Beukes, N., 2020a. The onset of oxidative weathering traced by uranium isotopes. Precambrian Res. 338, 105583.

Brüske, A., Weyer, S., Zhao, M.-Y., Planavsky, N., Wegwerth, A., Neubert, N., Dellwig, O., Lau, K., Lyons, T., 2020b. Correlated molybdenum and uranium isotope signatures in modern anoxic sediments: implications for their use as paleo-redox proxy. Geochim. Cosmochim. Acta 270, 449–474.

Calvert, S., Karlin, R., Toolin, L., Donahue, D., Southon, J., Vogel, J., 1991. Low organic carbon accumulation rates in Black Sea sediments. Nature 350 (6320), 692–695.

Canfield, D.E., Poulton, S.W., Knoll, A.H., Narbonne, G.M., Ross, G., Goldberg, T., Strauss, H., 2008. Ferruginous conditions dominated later neoproterozoic deep-water chemistry. Science 321 (5891), 949–952. https://doi.org/10.1126/science.1154499.

Cao, M., Daines, S.J., Lenton, T.M., Cui, H., Algeo, T.J., Dahl, T.W., Shi, W., Chen, Z.-Q., Anbar, A., Zhou, Y.-Q., 2020. Comparison of Ediacaran platform and slope δ238U records in South China: implications for global-ocean oxygenation and the origin of the Shuram Excursion. Geochim. Cosmochim. Acta 287, 111–124.

Chen, B., Hu, C., Mills, B.J., He, T., Andersen, M.B., Chen, X., Liu, P., Lu, M., Newton, R. J., Poulton, S.W., 2022. A short-lived oxidation event during the early Ediacaran and delayed oxygenation of the Proterozoic Ocean. Earth Planet. Sci. Lett. 577, 117274.

Chen, X., Ling, H.-F., Vance, D., Shields-Zhou, G.A., Zhu, M., Poulton, S.W., Och, L.M., Jiang, S.-Y., Li, D., Cremonese, L., 2015. Rise to modern levels of ocean oxygenation coincided with the Cambrian radiation of animals. Nat. Commun. 6.

Chen, X., Romaniello, S.J., Herrmann, A.D., Samankassou, E., Anbar, A.D., 2018. Biological effects on uranium isotope fractionation (238U/235U) in primary biogenic carbonates. Geochim. Cosmochim. Acta 240, 1–10. https://doi.org/10.1016/j.gca.2018.08.028.

Chen, X., Romaniello, S.J., Herrmann, A.D., Wasylenki, L.E., Anbar, A.D., 2016. Uranium isotope fractionation during coprecipitation with aragonite and calcite. Geochim. Cosmochim. Acta 188, 189–207.

Chen, X., Tissot, F., Jansen, M., Bekker, A., Liu, C., Nie, N., Halverson, G., Veizer, J., Dauphas, N., 2021. The uranium isotopic record of shales and carbonates through geologic time. Geochim. Cosmochim. Acta 300, 164–191.

Cheng, M., Li, C., Jin, C., Wang, H., Algeo, T.J., Lyons, T.W., Zhang, F., Anbar, A., 2020. Evidence for high organic carbon export to the early Cambrian seafloor. Geochim. Cosmochim. Acta 287, 125–140. https://doi.org/10.1016/j.gca.2020.01.050.

Chiu, C.F., Sweere, Tim C., Clarkson, Matthew O., de Souza, Gregory F., Hennekam, R., Vance, D., 2022. Co-variation systematics of uranium and molybdenum isotopes reveal pathways for descent into euxinia in Mediterranean sapropels. Earth Planet. Sci. Lett. 585.

Clark, S.K., Johnson, T.M., 2008. Effective isotopic fractionation factors for solute removal by reactive sediments: a laboratory microcosm and slurry study. Environ. Sci. Technol. 42 (21), 7850–7855.

Clarkson, M.O., Hennekam, R., Sweere, T.C., Andersen, M.B., Reichart, G.-J., Vance, D., 2021a. Carbonate associated uranium isotopes as a novel local redox indicator in oxidatively disturbed reducing sediments. Geochim. Cosmochim. Acta 311, 12–28.

Clarkson, M.O., Lenton, T.M., Andersen, M.B., Bagard, M.-L., Dickson, A.J., Vance, D., 2021b. Upper limits on the extent of seafloor anoxia during the PETM from uranium isotopes. Nat. Commun. 12 (1), 1–9.

Clarkson, M.O., Müsing, K., Andersen, M.B., Vance, D., 2020. Examining pelagic carbonate-rich sediments as an archive for authigenic uranium and molybdenum isotopes using reductive cleaning and leaching experiments. Chem. Geol. 539, 119412 https://doi.org/10.1016/j.chemgeo.2019.119412.

Clarkson, M.O., Stirling, C.H., Jenkyns, H.C., Dickson, A.J., Porcelli, D., Moy, C.M., von Strandmann, P.A.P., Cooke, I.R., Lenton, T.M., 2018. Uranium isotope evidence for two episodes of deoxygenation during Oceanic Anoxic Event 2. Proc. Natl. Acad. Sci. 115 (12), 2918–2923.

Cole, D.B., Planavsky, N.J., Longley, M., Böning, P., Wilkes, D., Wang, X., Swanner, E.D., Wittkop, C., Loydell, D.K., Busigny, V., 2020. Uranium isotope fractionation in non-sulfidic anoxic settings and the global uranium isotope mass balance. Glob. Biogeochem. Cycles 34 (8), e2020GB006649.

Dahl, T.W., Boyle, R.A., Canfield, D.E., Connelly, J.N., Gill, B.C., Lenton, T.M., Bizzarro, M., 2014. Uranium isotopes distinguish two geochemically distinct stages during the later Cambrian SPICE event. Earth Planet. Sci. Lett. 401, 313–326.

Dahl, T.W., Connelly, J., Kouchinsky, A., Gill, B., Månsson, S., Bizzarro, M., 2017. Reorganisation of Earth's biogeochemical cycles briefly oxygenated the oceans 520 Myr ago. Geochem. Perspect. 3, 210–220.

Dahl, T.W., Connelly, J.N., Li, D., Kouchinsky, A., Gill, B.C., Porter, S., Maloof, A.C., Bizzarro, M., 2019. Atmosphere–ocean oxygen and productivity dynamics during early animal radiations. Proc. Natl. Acad. Sci. 116 (39), 19352–19361.

Dang, D., Wang, W., Gibson, T., Kunzmann, M., Andersen, M., Halverson, G., Evans, R., 2022. Authigenic uranium isotopes of late Proterozoic black shale. Chem. Geol. 588, 120644.

Dang, D.H., Evans, R.D., Wang, W., Omanović, D., El Houssainy, A., Lenoble, V., Mullot, J.-U., Mounier, S., Garnier, C., 2018. Uranium isotope geochemistry in modern coastal sediments: Insights from Toulon Bay, France. Chem. Geol. 481, 133–145.

De Lange, G.J., Thomson, J., Reitz, A., Slomp, C.P., Principato, M.S., Erba, E., Corselli, C., 2008. Synchronous basin-wide formation and redox-controlled preservation of a Mediterranean sapropel. Nat. Geosci. 1 (9), 606–610.

De Rijk, S., Hayes, A., Rohling, E., 1999. Eastern Mediterranean sapropel S1 interruption: an expression of the onset of climatic deterioration around 7 ka BP. Mar. Geol. 153 (1–4), 337–343.

del Rey, Á., Havsteen, J.C., Bizzarro, M., Dahl, T.W., 2020. Untangling the diagenetic history of uranium isotopes in marine carbonates: a case study tracing the δ238U composition of late Silurian oceans using calcitic brachiopod shells. Geochim. Cosmochim. Acta 287, 93–110.

Dickson, A.J., Bagard, M.-L., Katchinoff, J.A.R., Davies, M., Poulton, S.W., Cohen, A.S., 2021. Isotopic constraints on ocean redox at the end of the Eocene. Earth Planet. Sci. Lett. 562, 116814 https://doi.org/10.1016/j.epsl.2021.116814.

Dunk, R., Mills, R., Jenkins, W., 2002. A reevaluation of the oceanic uranium budget for the Holocene. Chem. Geol. 190 (1), 45–67.

Elrick, M., Polyak, V., Algeo, T.J., Romaniello, S., Asmerom, Y., Herrmann, A.D., Anbar, A.D., Zhao, L., Chen, Z.-Q., 2017. Global-ocean redox variation during the middle-late Permian through early Triassic based on uranium isotope and Th/U trends of marine carbonates. Geology 45 (2), 163–166.

Gilleaudeau, G.J., Romaniello, S.J., Luo, G., Kaufman, A.J., Zhang, F., Klaebe, R.M., Kah, L.C., Azmy, K., Bartley, J.K., Zheng, W., 2019. Uranium isotope evidence for limited euxinia in mid-Proterozoic oceans. Earth Planet. Sci. Lett. 521, 150–157.

Grant, K., Grimm, R., Mikolajewicz, U., Marino, G., Ziegler, M., Rohling, E., 2016. The timing of Mediterranean sapropel deposition relative to insolation, sea-level and african monsoon changes. Quat. Sci. Rev. 140, 125–141.

Guilbaud, R., Poulton, S.W., Butterfield, N.J., Zhu, M., Shields-Zhou, G.A., 2015. A global transition to ferruginous conditions in the early Neoproterozoic oceans. advance online publication Nat. Geosci.. https://doi.org/10.1038/ngeo2434. http://www.nature.com/ngeo/journal/vaop/ncurrent/abs/ngeo2434.html#supplementary-information.

He, Z., Clarkson, M.O., Andersen, M.B., Archer, C., Sweere, T.C., Kraal, P., Guthauser, A., Huang, F., Vance, D., 2021. Temporally and spatially dynamic redox conditions on an upwelling margin: the impact on coupled sedimentary Mo and U isotope systematics, and implications for the Mo-U paleoredox proxy. Geochim. Cosmochim. Acta. https://doi.org/10.1016/j.gca.2021.06.024.

Hennekam, R., van der Bolt, B., van Nes, E.H., de Lange, G.J., Scheffer, M., Reichart, G.J., 2020. Early-warning signals for marine anoxic events. Geophys. Res. Lett. 47 (20), e2020GL089183.

Herrmann, A.D., Gordon, G.W., Anbar, A.D., 2018. Uranium isotope variations in a dolomitized Jurassic carbonate platform (Tithonian; Franconian Alb, Southern Germany). Chem. Geol. 497, 41–53.

Hinojosa, J.L., Stirling, C.H., Reid, M.R., Moy, C.M., Wilson, G.S., 2016. Trace metal cycling and 238U/235U in New Zealand's fjords: Implications for reconstructing global paleoredox conditions in organic-rich sediments. Geochim. Cosmochim. Acta 179, 89–109.

Holmden, C., Amini, M., Francois, R., 2015. Uranium isotope fractionation in Saanich Inlet: a modern analog study of a paleoredox tracer. Geochim. Cosmochim. Acta 153, 202–215.

Hood, A.V., Planavsky, N.J., Wallace, M.W., Wang, X., Bellefroid, E.J., Gueguen, B., Cole, D.B., 2016. Integrated geochemical-petrographic insights from component-selective δ238U of Cryogenian marine carbonates. Geology 44 (11), 935–938.

Jost, A.B., Bachan, A., van de Schootbrugge, B., Lau, K.V., Weaver, K.L., Maher, K., Payne, J.L., 2017. Uranium isotope evidence for an expansion of marine anoxia during the end-Triassic extinction. Geochem. Geophys. Geosyst. 18, 3093–3108.

Kendall, B., Komiya, T., Lyons, T.W., Bates, S.M., Gordon, G.W., Romaniello, S.J., Jiang, G., Creaser, R.A., Xiao, S., McFadden, K., 2015. Uranium and molybdenum isotope evidence for an episode of widespread ocean oxygenation during the late Ediacaran Period. Geochim. Cosmochim. Acta 156, 173–193.

Kendall, B., Wang, J., Zheng, W., Romaniello, S.J., Over, D.J., Bennett, Y., Xing, L., Kunert, A., Boyes, C., Liu, J., 2020. Inverse correlation between the molybdenum and uranium isotope compositions of Upper Devonian black shales caused by changes in local depositional conditions rather than global ocean redox variations. Geochim. Cosmochim. Acta 287, 141–164.

Kipp, M.A., Tissot, F.L., 2022. Inverse methods for consistent quantification of seafloor anoxia using uranium isotope data from marine sediments. Earth Planet. Sci. Lett. 577, 117240.

Lau, K.V., Hancock, L.G., Severmann, S., Kuzminov, A., Cole, D.B., Behl, R.J., Planavsky, N.J., Lyons, T.W., 2022. Variable local basin hydrography and productivity control the uranium isotope paleoredox proxy in anoxic black shales. Geochim. Cosmochim. Acta 317, 433–456. https://doi.org/10.1016/j.gca.2021.10.011.

Lau, K.V., Lyons, T.W., Maher, K., 2020. Uranium reduction and isotopic fractionation in reducing sediments: Insights from reactive transport modeling. Geochim. Cosmochim. Acta 287, 65–92.

Lau, K.V., Macdonald, F.A., Maher, K., Payne, J.L., 2017. Uranium isotope evidence for temporary ocean oxygenation in the aftermath of the Sturtian Snowball Earth. Earth Planet. Sci. Lett. 458, 282–292.

Lau, K.V., Maher, K., Altiner, D., Kelley, B.M., Kump, L.R., Lehrmann, D.J., Silva-Tamayo, J.C., Weaver, K.L., Yu, M., Payne, J.L., 2016. Marine anoxia and delayed Earth system recovery after the end-Permian extinction. Proc. Natl. Acad. Sci. 113 (9), 2360–2365.

Li, C., Love, G.D., Lyons, T.W., Fike, D.A., Sessions, A.L., Chu, X., 2010. A stratified redox model for the Ediacaran Ocean. Science 328 (5974), 80–83.

Li, Z., Cao, M., Loyd, S.J., Algeo, T.J., Zhao, H., Wang, X., Zhao, L., Chen, Z.-Q., 2020. Transient and stepwise ocean oxygenation during the late Ediacaran Shuram Excursion: Insights from carbonate δ238U of northwestern Mexico. Precambrian Res. 344, 105741.

Lyons, T.W., Diamond, C.W., Planavsky, N.J., Reinhard, C.T., Li, C., 2021. Oxygenation, life, and the planetary system during Earth's middle history: an overview. Astrobiology 21 (8), 906–923.

Lyons, T.W., Reinhard, C.T., Planavsky, N.J., 2014. The rise of oxygen in Earth's early ocean and atmosphere. Nature 506 (7488), 307–315.

Matthews, A., Azrieli-Tal, I., Benkovitz, A., Bar-Matthews, M., Vance, D., Poulton, S.W., Teutsch, N., Almogi-Labin, A., Archer, C., 2017. Anoxic development of sapropel S1 in the Nile Fan inferred from redox sensitive proxies, Fe speciation, Fe and Mo isotopes. Chem. Geol. 475, 24–39.

McDonald, B.S., Partin, C.A., Sageman, B., Holmden, C., 2022. Uranium isotope reconstruction of ocean deoxygenation during OAE 2 hampered by uncertainties in fractionation factors and local U-cycling. Geochim. Cosmochim. Acta 331, 143–164.

McLennan, S.M., 2001. Relationships between the trace element composition of sedimentary rocks and upper continental crust. Geochem. Geophys. Geosyst. 2 (4).

McManus, J., Berelson, W.M., Severmann, S., Poulson, R.L., Hammond, D.E., Klinkhammer, G.P., Holm, C., 2006. Molybdenum and uranium geochemistry in continental margin sediments: paleoproxy potential. Geochim. Cosmochim. Acta 70 (18), 4643–4662.

Montoya-Pino, C., Weyer, S., Anbar, A.D., Pross, J., Oschmann, W., van de Schootbrugge, B., Arz, H.W., 2010. Global enhancement of ocean anoxia during Oceanic Anoxic Event 2: a quantitative approach using U isotopes. Geology 38 (4), 315–318.

Neubert, N., Nägler, T.F., Böttcher, M.E., 2008. Sulfidity controls molybdenum isotope fractionation into euxinic sediments: evidence from the modern Black Sea. Geology 36 (10), 775–778.

Noordmann, J., Weyer, S., Georg, R.B., Jöns, S., Sharma, M., 2015a. 238U/235U isotope ratios of crustal material, rivers and products of hydrothermal alteration: new insights on the oceanic U isotope mass balance. Isot. Environ. Health Stud. 1–23.

Noordmann, J., Weyer, S., Montoya-Pino, C., Dellwig, O., Neubert, N., Eckert, S., Paetzel, M., Böttcher, M., 2015b. Uranium and molybdenum isotope systematics in modern euxinic basins: Case studies from the Central Baltic Sea and the Kyllaren fjord (Norway). Chem. Geol. 396, 182–195.

Och, L.M., Cremonese, L., Shields-Zhou, G.A., Poulton, S.W., Struck, U., Ling, H., Li, D., Chen, X., Manning, C., Thirlwall, M., Strauss, H., Zhu, M., 2016. Palaeoceanographic controls on spatial redox distribution over the Yangtze Platform during the Ediacaran-Cambrian transition. Sedimentology 63 (2), 378–410. https://doi.org/10.1111/sed.12220.

Pogge von Strandmann, P.A., Stüeken, E.E., Elliott, T., Poulton, S.W., Dehler, C.M., Canfield, D.E., Catling, D.C., 2015. Selenium isotope evidence for progressive oxidation of the Neoproterozoic biosphere. Nat. Commun. 6 (1), 1–10.

Poulton, S.W., Canfield, D.E., 2011. Ferruginous Conditions: a Dominant Feature of the Ocean through Earth's history. Elements 7 (2), 107–112. https://doi.org/10.2113/gselements.7.2.107.

Reitz, A., Wille, M., Nägler, T.F., de Lange, G.J., 2007. Atypical Mo isotope signatures in eastern Mediterranean sediments. Chem. Geol. 245 (1–2), 1–8.

Rohling, E., Marino, G., Grant, K., 2015. Mediterranean climate and oceanography, and the periodic development of anoxic events (sapropels). Earth Sci. Rev. 143, 62–97.

Rohling, E., Mayewski, P., Abu-Zied, R., Casford, J., Hayes, A., 2002. Holocene atmosphere-ocean interactions: records from Greenland and the Aegean Sea. Clim. Dyn. 18 (7), 587–593.

Rolison, J.M., Stirling, C.H., Middag, R., Rijkenberg, M.J.A., 2017. Uranium stable isotope fractionation in the Black Sea: Modern calibration of the 238U/235U paleoredox proxy. Geochim. Cosmochim. Acta 203, 69–88.

Romaniello, S.J., Herrmann, A.D., Anbar, A.D., 2013. Uranium concentrations and 238U/235U isotope ratios in modern carbonates from the Bahamas: Assessing a novel paleoredox proxy. Chem. Geol. 362, 305–316. https://doi.org/10.1016/J.Chemgeo.2013.10.002.

Sahoo, S.K., Planavsky, N., Jiang, G., Kendall, B., Owens, J., Wang, X., Shi, X., Anbar, A., Lyons, T., 2016. Oceanic oxygenation events in the anoxic Ediacaran Ocean. Geobiology 14 (5), 457–468.

Scholz, F., Hensen, C., Noffke, A., Rohde, A., Liebetrau, V., Wallmann, K., 2011. Early diagenesis of redox-sensitive trace metals in the Peru upwelling area–response to ENSO-related oxygen fluctuations in the water column. Geochim. Cosmochim. Acta 75 (22), 7257–7276.

Scott, C., Lyons, T.W., 2012. Contrasting molybdenum cycling and isotopic properties in euxinic versus non-euxinic sediments and sedimentary rocks: refining the paleoproxies. Chem. Geol. 324–325, 19–27. https://doi.org/10.1016/j.chemgeo.2012.05.012.

Shi, W., Mills, B.J.W., Li, C., Poulton, S.W., Krause, A.J., He, T., Zhou, Y., Cheng, M., Shields, G.A., 2022. Decoupled oxygenation of the Ediacaran Ocean and atmosphere during the rise of early animals. Earth Planet. Sci. Lett. 591, 117619 https://doi.org/10.1016/j.epsl.2022.117619.

Shields, G.A., Mills, B.J., Zhu, M., Raub, T.D., Daines, S.J., Lenton, T.M., 2019. Unique Neoproterozoic carbon isotope excursions sustained by coupled evaporite dissolution and pyrite burial. Nat. Geosci. 12 (10), 823–827.

Song, H., Song, H., Algeo, T.J., Tong, J., Romaniello, S.J., Zhu, Y., Chu, D., Gong, Y., Anbar, A.D., 2017. Uranium and carbon isotopes document global-ocean redox-productivity relationships linked to cooling during the Frasnian-Famennian mass extinction. Geology 45 (10), 887–890.

Sperling, E.A., Wolock, C.J., Morgan, A.S., Gill, B.C., Kunzmann, M., Halverson, G.P., Macdonald, F.A., Knoll, A.H., Johnston, D.T., 2015. Statistical analysis of iron geochemical data suggests limited late Proterozoic oxygenation. Nature 523 (7561), 451–454. https://doi.org/10.1038/nature14589.

Stirling, C.H., Andersen, M.B., Warthmann, R., Halliday, A.N., 2015. Isotope fractionation of 238U and 235U during biologically-mediated uranium reduction. Geochim. Cosmochim. Acta 163, 200–218.

Stockey, R.G., Cole, D.B., Planavsky, N.J., Loydell, D.K., Frýda, J., Sperling, E.A., 2020. Persistent global marine euxinia in the early Silurian. Nat. Commun. 11 (1), 1–10.

Stylo, M., Neubert, N., Wang, Y., Monga, N., Romaniello, S.J., Weyer, S., Bernier-Latmani, R., 2015. Uranium isotopes fingerprint biotic reduction. Proc. Natl. Acad. Sci. 112 (18), 5619–5624.

Sweere, T., Hennekam, R., Vance, D., Reichart, G.J., 2021. Molybdenum isotope constraints on the temporal development of sulfidic conditions during Mediterranean sapropel intervals. Geochem. Perspect. Lett. 17, 16–20. https://doi.org/10.7185/geochemlet.2108.

Taylor, S.R., McLennan, S.M., 1985. The continental crust: its composition and evolution.

Tostevin, R., Clarkson, M.O., Gangl, S., Shields, G.A., Wood, R.A., Bowyer, F., Penny, A. M., Stirling, C.H., 2019. Uranium isotope evidence for an expansion of anoxia in terminal Ediacaran oceans. Earth Planet. Sci. Lett. 506, 104–112.

Tostevin, R., Mills, B.J., 2020. Reconciling proxy records and models of Earth's oxygenation during the Neoproterozoic and Palaeozoic. Interf. Focus 10 (4), 20190137.

Tostevin, R., Wood, R.A., Shields, G.A., Poulton, S.W., Guilbaud, R., Bowyer, F., Penny, A.M., He, T., Curtis, A., Hoffmann, K.H., Clarkson, M.O., 2016. Low-oxygen waters limited habitable space for early animals, 7. https://www.nature.com/articles/ncomms12818#supplementary-information.

Tribovillard, N., Algeo, T.J., Lyons, T., Riboulleau, A., 2006. Trace metals as paleoredox and paleoproductivity proxies: an update. Chem. Geol. 232 (1–2), 12–32.

Wei, G.-Y., Planavsky, N.J., He, T., Zhang, F., Stockey, R.G., Cole, D.B., Lin, Y.-B., Ling, H.-F., 2021. Global marine redox evolution from the late Neoproterozoic to the early Paleozoic constrained by the integration of Mo and U isotope records. Earth Sci. Rev. 214, 103506 https://doi.org/10.1016/j.earscirev.2021.103506.

Wei, G.-Y., Planavsky, N.J., Tarhan, L.G., Chen, X., Wei, W., Li, D., Ling, H.-F., 2018. Marine redox fluctuation as a potential trigger for the Cambrian explosion. Geology 46 (7), 587–590.

Wei, G.-Y., Planavsky, N.J., Tarhan, L.G., He, T., Wang, D., Shields, G.A., Wei, W., Ling, H.-F., 2020. Highly dynamic marine redox state through the Cambrian explosion highlighted by authigenic δ238U records. Earth Planet. Sci. Lett. 544, 116361 https://doi.org/10.1016/j.epsl.2020.116361.

Weyer, S., Anbar, A., Gerdes, A., Gordon, G., Algeo, T., Boyle, E., 2008. Natural fractionation of 238U/235U. Geochim. Cosmochim. Acta 72 (2), 345–359.

White, D.A., Elrick, M., Romaniello, S., Zhang, F., 2018. Global seawater redox trends during the late Devonian mass extinction detected using U isotopes of marine limestones. Earth Planet. Sci. Lett. 503, 68–77.

Wood, R., Liu, A.G., Bowyer, F., Wilby, P.R., Dunn, F.S., Kenchington, C.G., Cuthill, J.F. H., Mitchell, E.G., Penny, A., 2019. Integrated records of environmental change and evolution challenge the Cambrian Explosion. Nat. Ecol. Evol. 3 (4), 528–538.

Wood, R.A., Poulton, S.W., Prave, A.R., Hoffmann, K.H., Clarkson, M.O., Guilbaud, R., Lyne, J.W., Tostevin, R., Bowyer, F., Penny, A.M., Curtis, A., Kasemann, S.A., 2015. Dynamic redox conditions control late Ediacaran metazoan ecosystems in the Nama Group, Namibia. Precambrian Res. 261, 252–271. https://doi.org/10.1016/j.precamres.2015.02.004.

Yang, C., Rooney, A.D., Condon, D.J., Li, X.-H., Grazhdankin, D.V., Bowyer, F.T., Hu, C., Macdonald, F.A., Zhu, M., 2021. The tempo of Ediacaran evolution. Sci. Adv. 7 (45), eabi9643.

Yiğiterhan, O., Murray, J.W., 2008. Trace metal composition of particulate matter of the Danube River and turkish rivers draining into the Black Sea. Mar. Chem. 111 (1), 63–76. https://doi.org/10.1016/j.marchem.2007.06.019.

Zhang, F., Algeo, T.J., Romaniello, S.J., Cui, Y., Zhao, L., Chen, Z.-Q., Anbar, A.D., 2018a. Congruent Permian-Triassic δ238U records at Panthalassic and Tethyan sites: Confirmation of global-oceanic anoxia and validation of the U-isotope paleoredox proxy. Geology 46 (4), 327–330.

Zhang, F., Dahl, T.W., Lenton, T.M., Luo, G., Shen, S.-Z., Algeo, T.J., Planavsky, N., Liu, J., Cui, Y., Qie, W., 2020a. Extensive marine anoxia associated with the late Devonian Hangenberg Crisis. Earth Planet. Sci. Lett. 533, 115976.

Zhang, F., Lenton, T.M., del Rey, Á., Romaniello, S.J., Chen, X., Planavsky, N.J., Clarkson, M.O., Dahl, T.W., Lau, K.V., Wang, W., 2020b. Uranium isotopes in marine carbonates as a global ocean paleoredox proxy: a critical review. Geochim. Cosmochim. Acta 287, 27–49.

Zhang, F., Romaniello, S.J., Algeo, T.J., Lau, K.V., Clapham, M.E., Richoz, S., Herrmann, A.D., Smith, H., Horacek, M., Anbar, A.D., 2018b. Multiple episodes of extensive marine anoxia linked to global warming and continental weathering following the latest Permian mass extinction. Sci. Adv. 4 (4), e1602921.

Zhang, F., Shen, S.-Z., Cui, Y., Lenton, T.M., Dahl, T.W., Zhang, H., Zheng, Q.-F., Wang, W., Krainer, K., Anbar, A.D., 2020c. Two distinct episodes of marine anoxia during the Permian-Triassic crisis evidenced by uranium isotopes in marine dolostones. Geochim. Cosmochim. Acta 287, 165–179.

Zhang, F., Stockey, R.G., Xiao, S., Shen, S.-Z., Dahl, T.W., Wei, G.-Y., Cao, M., Li, Z., Kang, J., Cui, Y., Anbar, A.D., Planavsky, N.J., 2022. Uranium isotope evidence for extensive shallow water anoxia in the early Tonian oceans. Earth Planet. Sci. Lett. 583, 117437 https://doi.org/10.1016/j.epsl.2022.117437.

Zhang, F., Xiao, S., Kendall, B., Romaniello, S.J., Cui, H., Meyer, M., Gilleaudeau, G.J., Kaufman, A.J., Anbar, A.D., 2018c. Extensive marine anoxia during the terminal Ediacaran Period. Sci. Adv. 4 (6), eaan8983.

Zhang, F., Xiao, S., Romaniello, S.J., Hardisty, D., Li, C., Melezhik, V., Pokrovsky, B., Cheng, M., Shi, W., Lenton, T.M., 2019. Global marine redox changes drove the rise and fall of the Ediacara biota. Geobiology 17 (6), 594–610.

Zheng, Y., Anderson, R.F., van Geen, A., Fleisher, M.Q., 2002. Preservation of particulate non-lithogenic uranium in marine sediments. Geochim. Cosmochim. Acta 66 (17), 3085–3092.